Lithium aluminum alloy anodes in Li-ion rechargeable batteries: past developments, recent progress, and future prospects

To cite this article: Tianye Zheng and Steven T Boles 2023 *Prog. Energy* **5** 032001

IOP Publishing Prog. Energy 5 (2023) 032001 https://doi.org/10.1088/2516-1083/acd101

Progress in Energy

OPEN ACCESS

RECEIVED
17 February 2023

REVISED
27 March 2023

ACCEPTED FOR PUBLICATION
27 April 2023

PUBLISHED
17 May 2023

TOPICAL REVIEW

Lithium aluminum alloy anodes in Li-ion rechargeable batteries: past developments, recent progress, and future prospects

Tianye Zheng[1,2,*] and **Steven T Boles**[1,3,4,*]

[1] Department of Electrical Engineering, The Hong Kong Polytechnic University, Hung Hom, Kowloon, Hong Kong Special Administrative Region of China, People's Republic of China
[2] Photonics Research Institute, The Hong Kong Polytechnic University, Hung Hom, Kowloon, Hong Kong Special Administrative Region of China, People's Republic of China
[3] Department of Energy and Process Engineering, Norwegian University of Science and Technology, Høgskoleringen 1, 7491 Trondheim, Norway
[4] Centre for Advances in Reliability and Safety (CAiRS), Hong Kong Science Park, New Territories, Hong Kong Special Administrative Region of China, People's Republic of China
[*] Authors to whom any correspondence should be addressed.

E-mail: darren.ty.zheng@connect.polyu.hk and steven.boles@ntnu.no

Keywords: lithium-ion batteries, lithium-aluminum alloys, phase transformations, temperature effects, safety concerns, solid-state cells, strategic utilization

Supplementary material for this article is available online

Abstract

Aluminum (Al) metal has long been known to function as an anode in lithium-ion batteries (LIBs) owing to its high capacity, low potential, and effective suppression of dendrite growth. However, seemingly intrinsic degradation during cycling has made it less attractive throughout the years compared to graphitic carbon, silicon-blends, and more recently lithium metal itself. Nevertheless, with the recent unprecedented growth of the LIB industry, this review aims to revisit Al as an anode material, particularly in light of important advancements in understanding the electrochemical Li-Al system, as well as the growth of activity in solid-state batteries where cell designs may conveniently mitigate problems found in traditional liquid cells. Furthermore, this review culminates by highlighting several non-trivial points including: (1) prelithiatied Al anodes, with β-LiAl serving as an intercalation host, can be effectively immortal, depending on formation and cycling conditions; (2) the common knowledge of Al having a capacity of 993 mAh g^{-1} is inaccurate and attributed to kinetic limitations, thus silicon and lithium should not stand alone as the only 'high-capacity' candidates in the roadmap for future lithium-ion cells; (3) replacement of Cu current collectors with Al-based foil anodes may simplify LIB manufacturing and has important safety implications due to the galvanic stability of Al at high potentials vs. Li/Li^+. Irrespective of the type of Li-ion device of interest, this review may be useful for those in the broader community to enhance their understanding of general alloy anode behavior, as the methodologies reported here can be extended to non-Al anodes and consequently, even to Na-ion and K-ion devices.

Contents

1. Introduction

Whether driven by the desire for a shift to renewable energy sources, or by geopolitical instabilities, improved energy storage technologies are unambiguously poised to play a critical role in a decarbonized world. The coincidental timing of a global energy crisis (1970s) with the emergence of consumer portable electronics (1980s) would spur the development of an interest in electrochemical energy storage with performance characteristics that were previously unheard of. Owing to its atomic arrangement, lithium-based cells are inevitably at the forefront of the push towards batteries with the highest power densities and best specific capacities. Nevertheless, despite the past ~50 years of continued advancements for lithium-ion batteries (LIBs), a commitment to developing next-generation Li-based cells with largely enhanced energy/power densities is warranted as these devices are only now seeing the widespread adoption in electric vehicles (EVs) and energy storage systems that are poised to lead to societal transformation [1]. Interestingly, even though excitement abounds for the 'next-generation' of devices, a dichotomy has evolved between industry and academia, with the former taking a ruthlessly conservative approach to innovating a commodity, whilst the latter pushes to the bleeding edge of innovation with constant technological advancements, but is also

plagued with science fiction [2, 3], made worse by winner-take-all and beauty pageant resource allocation [4]. With this in mind, it is essential to first reconcile LIB design thinking between these two groups, prior to discussing the topic at hand.

1.1. Current situation of LIBs

In industry, the capacity of a commercial LIB full cell is restricted by the cathode mass while the anode will be scaled to deliver about 1.1 times this capacity (i.e. an N-to-P ratio of ∼1.1), so as to avoid the risk of lithium deposition at 100% state of charge. In other words, only the mass loading (mass/thickness over the surface area) of the cathode is adjusted to compromise the desired energy density and determines the cell size. Applying this process to the format of an exemplary 18650-battery cell, although more cathode mass would result in higher cell energy, the composite-based nature of the electrode design limits its thickness to (usually) the scale of ∼100 μm. Eventually, the jelly roll including both electrodes, current collectors, separators, and additives, must fit into a cylindrical stainless-steel case with 18 mm in diameter and 65 mm in height. Importantly, the volume of the jelly roll should be slightly smaller than the case, e.g. ∼2% of the volume is reserved to allow some degree of jelly roll expansion, and thus helps to ensure safe operations. Overall, one can notice that the process and forms of the anode and cathode are closely linked in LIB full cell during manufacturing.

In academia, on the other hand, research in anode and cathode materials is usually isolated to gain scientific insights in a better way. For instance, a half-cell configuration of anode vs. Li metal eliminates any possible influences, noises, or complications arising from a cathode (and vice versa). Three-electrode reference cells can overcome such challenges when a full cell is in use, but these require a more expensive potentiostat, rather than simple battery cycling hardware, as well as the discrete integration of a third electrode with a stable electrochemical potential. Thus, an awkward situation can arise where some researchers with expertise in either anode or cathode may have different opinions in defining criteria for a full cell as a device. The phenomena can be realized by noting that many studies have been focusing on maximizing the anode capacity and reporting some of the highest figures in mAh g^{-1} while the cathode capacity is still substantially limited by its layered structures and intercalation chemistry. High mAh g^{-1} numbers for the anode will necessitate large volume expansion (ca. 12.9 cm^3 mol^{-1} Li), regardless of host materials (figure 1(a)) [5, 6], but high voltage cathode materials will not expand congruently. M. N. Obrovac had developed a model to estimate the energy of $LiCoO_2$ cells with various anode materials, highlighting that replacing graphite anode with Si (potentially stores 22.5 times more Li) would lead to merely an optimum 34% (⩽20% in reality due to pores and nanostructures) increase in cell energy due to the volume expansion mentioned above [6, 7]. Therefore, a cell's package must accommodate volume expansion and contraction with every cycle, and this is proving to be exceedingly concerning at all levels of development (for example with SEI formation on fresh anode surfaces inside each cell, or with cell level expansion leading to mechanical stress and module level deformation).

Accordingly, one must reconsider whether achieving the highest specific capacity figures should be the top priority for research in the area of anode materials for LIBs. Given the diminishing returns when pursuing increasingly costly and complex anode architectures, ideal anodes in LIBs should be expected to balance the cost, capacity, and manufacturing complexity for every application [11, 12], with the specter of sustainability looming large over every material, process, and geographic source. Thus, a revisitation of anode-free, lithium-metal batteries is certainly warranted since the many problems from the first generation of lithium-metal batteries can be alleviated if these designs can be realized [13]. However, it is far from clear whether or not lithium deposition can be reversibly achieved with Frank–van der Merwe growth and thin/thick-film formation, in the absence of a template or secondary substrate, irrespective of whether it is a liquid or solid-state cell. In the end, what companies adopt in the future as their LIB anodes is still largely unclear, with different considerations leading to different opinions (not surprising).

Current state-of-the-art anode designs in liquid cells are composite-based, consisting of active materials, polymer/organic binders, and electrical conductivity enhancers, all in powder form. Solvents are used to create a homogeneous mixture that is subsequently pasted on a piece of Cu foil before it is subject to baking, calendering, and cell assemblies. Interestingly, in academic discussions, specific capacity in mAh g^{-1} is often normalized to mere active material mass (>95% in industry, but often ∼70% to 80% in academia), with the binder and additives being excluded, and of course, the mass of current collector foils being neglected as well. It then leaves little surprise that silicon, among all anode candidates, receives extraordinary attention due to a theoretical specific capacity as high as ∼3579 mAh g^{-1}, with abundant literature [14–24] and cumulative funding passing the USD 2B threshold [25]. Yet, the huge volume changes of Si associated with Li insertion/extraction (>300%) still prevent pure Si anodes from being successfully commercialized

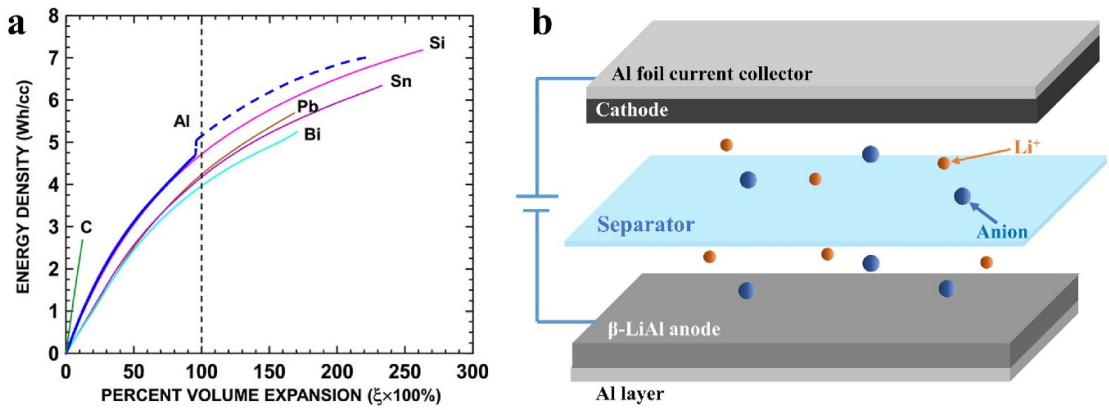

Figure 1. (a) The energy expansion curves (paired with a 3.75 V vs. Li/Li^+ cathode) for various anode materials calculated from their voltage curves. The dashed line extended from the Al curve is an extrapolation that indicates the Li_9Al_4 formation, where the Li solubility range of β-LiAl is reflected by the kink. The β-LiAl can store/release a certain amount of Li without altering its crystal structure, and thus giving a small volume change (e.g. ∼1.4%) [9]. Reproduced from [8]. [© 2007 ECS - The Electrochemical Society]. All rights reserved. (b) A schematic illustration of LIB cells when conventional anodes are replaced by Al foil anodes. Reproduced from [10]. CC BY 4.0.

(admittedly a controversial, but defensible statement). At the industrial scale, compromise has been made to mix high-capacity Si or SiO_x alloy powders with conventional graphite as additives (e.g. usually $\leqslant$ 20%), such that the volume change is acceptable while the energy density can be increased to some extent [26–32].

Recently, the concept of using metallic foils has regained interest as the negative electrode for LIB cells amongst some in the academic community [5, 33–35]. The concept of using foil anodes is to omit the usage of binders, Cu foils, etc., and to skip the mixing/baking steps. Not only can the material cost be reduced by occupying fewer chemicals/components, but also the multi-step nature of the anode fabrication can potentially be simplified [10]. When Cu foil no longer exists in LIB cells, its risk of being oxidized or even dissolved, which could lead to internal short-circuit at over-discharging states (e.g. 0 V for a full cell), is also eliminated. Heligman and Manthiram have tested 16 different metallic foils and concluded that In, Sn, and Al foils deliver promising capacities as well as formation efficiencies [36]. Some successful demonstrations of In foil [37, 38], Sn foil [39–43], and Al foil anodes [43–48] can also support their conclusions. Novel alloy strategies using interdigitated eutectic alloys may further be a way to utilize one or more active metals, whilst maintaining some structural supporting matrix [39, 49]. Impressively, some of those foil anodes achieved performances that can compete with or even surpass the composite ones, validating the idea that the future LIB anodes may be entirely solid-state in the form of a simple metal or metal alloy, regardless of the state of electrolyte (i.e. solid or liquid). A simple illustration is given in figure 1(b) to describe the internal structure of a LIB cell which consists of the Al foil anode instead of the conventional one. Although thick foils may sacrifice a certain degree of flexibility, the design can readily be used in prismatic cells. Importantly, the illustrated electrode stack may be extremely suitable for the bipolar design [50], which minimizes the weight/volume occupied by cell packaging, thereby improving the gravimetric/volumetric energy densities. Lastly, this simple foil architechture is suggested to possess great potential in making the future LIBs completely solid state if the cathodes made from solid foil ceramic−metal composites are envisioned.

From a practical perspective, it is also necessary to consider how an anode performs under more extreme testing conditions, particularly with respect to environmental considerations such as temperature and pressure. With electric vehicle adoption being widespread across the globe, cells will be exposed to −10 °C to 50 °C ambient variations which are likely beyond the stable operating range for many electrochemical devices, not just batteries. Therefore, the introduction of thermal stability control is essential. For instance, when the battery pack of Tesla EVs heats up to 55 °C, the built-in cooling system is activated. It is believed that slightly higher temperatures above ambient are preferred, which facilitate a faster ion diffusion (i.e. faster charging), and help reduce the ohmic loss that could lead to thermodynamically favorable conditions for lithium plating, but what is this ideal temperature for ensuring rapid charging and optimal safety at the same time? In the case of carbon anodes and carbonate electrolytes, 50 °C may indeed be ideal, and operation at such a moderately elevated temperature warrants further consideration for any new materials.

High-pressure situations are also effectively intrinsic for both liquid cells and solid-state batteries. Commonly, liquid cells will be stacked and assembled into modules under significant compressive force. With swelling and internal expansion with fixed volumes, compressive stress is inevitable. In the solid-state

case, ion migration will be accompanied by continuous structural rearrangement, but to what extent stress helps to reduce the likelihood of lithium dendrite formation is still unclear [51]. Furthermore, compressive stress comes at a significant cost in LIB anode materials. Sethuraman *et al* highlighted how the effective lithiation potential of silicon is shifted according to the extent of applied stress [52]. While 60 mV GPa^{-1} may seem insignificant, 50 MPa of external stack pressure on a solid-state battery could readily translate into a stress level that is several orders of magnitude higher between particles in powder-based electrodes and electrolytes. When coupled with internal stresses during lithiation, it can be expected to significantly change the scenario for the effective capacity of the selected anode material. Furthermore, in a solid-state cell, Li-ion transport is restricted to solids and interfaces which have been notoriously complex to understand, let alone optimize. For an anode material, volume expansion and phase transformations are both necessary to have a low potential and optimized specific energy density. An optimization between thermodynamic and kinetic performance should be expected and the classical interrelations between structure-process-property and performance will be as interlinked as ever.

1.2. Aluminum (Al) as an anode material

Al, as a well-known engineering material, can be found everywhere in our daily lives from aviation applications to food/beverage packaging and already functions as the cathode current collector and pouch cell case in LIBs. Historically, the Al alloy anode was introduced in the early 1970s to replace Li metal since it was found by Exxon that a LiAl alloy could effectively suppress the growth of Li dendrites on its surface [53]. This cell design was the predecessor of LIB where both the anode and cathode serve as Li hosts with no metallic Li present. Attempts had been made to commercialize Al anodes with some success but the discovery of graphite as a negative electrode by Yazami and Touzain in 1983 would effectively mute such pursuits [54]. Later Yoshino's team put together the graphite anode and the $LiCoO_2$ cathode in 1985 and officially named it a LIB [55]. Since then, the research focus on anodes had been shifted from LiAl alloy to carbon-based one (graphite) and eventually triggered the successful commercialization and popularization of LIBs.

Despite the growth of carbon as the choice for Sony's LIB anodes, some interests remained in Al or Al-alloys. In the 1990s, Li-Al alloys with just 6% depth of discharge were reported to last for 250 cycles with failure attributed to nonuniform reactions between Li and Al and fine particle formation (i.e. pulverization) [56]. Additives of Mn or Cr were introduced to extend the lifetime to 500 cycles, but challenges with complete capacity utilization remained. Pushing towards full cycling performance with Al metal anodes, it is common that electrode lifetimes of only a dozen of cycles are reported [57–62]. The underlying reasons behind the drastic capacity fading at room temperature vary a bit and include (but are not limited to): (1) the $\sim$95% expansion in lattice volume per Al unit cell (face-centered cubic; fcc) upon lithiation [63]; (2) the mechanical brittleness of the lithiated phases [64]; (3) heterogeneous nucleation with unequally distributed interfacial strain [65, 66]; (4) formation of nanopores/voids after β-to-α phase transformation [67, 68]; (5) lithium trapping issues [59]. Nevertheless, a few studies can still demonstrate the reasonable cycling of Al anodes [43–45]. The dichotomy between excellent and poor cycling performance is well captured by examining the Maxell ML series lithium-ion cells. The $LiMnO_2$-Al cell utilizes an Al foil with a surface pattern for the anode, and according to the product datasheet in figure 2, can cycle over 10^3 times if the depth of discharge is kept below $\sim$10%. However, if the depth of discharge is pushed to $>$80%, barely a handful of cycles can be expected prior to failure.

In the public domain, the origin of the anomalously good performance of Li-ion cells with Al anodes is somewhat of a mystery, and even though several tens of review articles of Si-based anodes can be easily accessed, a comprehensive picture of the evolution and lithium pathways in Al anodes can hardly be found [70]. Perhaps partly due to this situation, Al is still not considered a promising anode candidate for LIB cells. With this report, the authors aim at achieving a unified understanding of why Al anodes often degrade very quickly but sometimes seem to be reliable, by summarizing the available literature and supplementing with our own previously unpublished work (where appropriate). Not only is the recent progress on Al-based anodes for LIB applications highlighted, but some excellent studies published several decades ago are also acknowledged to provide a comprehensive picture of the topic. We have attempted to write this article in a systematic fashion starting with (§ 2) fundamentals in the binary Li-Al system, explaining the origin of the Al anode capacity from a metallurgic point of view. Then (§ 3) the electrochemical lithiation of Al and (§ 4) delithiation of Li-Al alloys. This is subsequently expanded (§ 5) to consider long-term cycling and (§ 6) important scenarios for operation and usage including anode effective-immortality, moderately elevated temperature operation, and implementation in solid-state cells. Although we have tried to adequately cover the range of contributors to this field, we humbly apologize in advance for any references overlooked or omitted, as this is purely unintentional considering our focus on the Li-Al electrochemical system as it pertains to LIB anodes, as opposed to providing a comprehensive overview of the numerous works in this area.

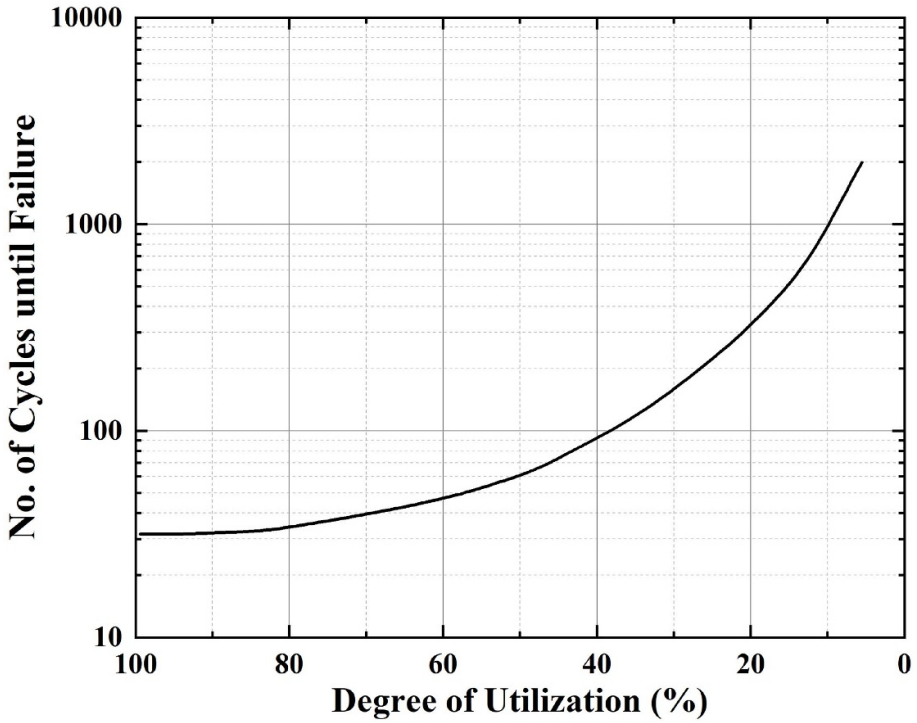

Figure 2. Cycling guide of Maxell ML series $LiMnO_2$-Al cells, modeled after their official product datasheet [69]. The degree of utilization refers to the percentage of Al foil being utilized for storing Li.

2. Fundamentals of the Li-Al system

Firstly, the physio-chemical properties of Li-Al alloys should be discussed from the perspectives of metallurgy and material sciences, followed by an introduction to their electrochemical nature.

2.1. Li-Al binary phase diagram

Al can form various alloys with Li, as shown in the phase diagrams published in the 1980s [71, 72]. Later a new phase ($Li_{2-x}Al$; orthorhombic) was identified and this was included in the range of compounds that can be formed by the two elements not long ago [73]. By summarizing the literature, a modified phase diagram is given in figure 3, with a specific emphasize on the temperatures from ambient to 350 °C, which should cover the common operation conditions for LIBs. Based on their atomic ratios, these lithiated phases may be expected to give very attractive capacities of ~993 mAh g^{-1}, ~1490 mAh g^{-1}, ~1986 mAh g^{-1}, and ~2234 mAh g^{-1} for the formations of β-LiAl, Li_3Al_2, $Li_{2-x}Al$, and Li_9Al_4, respectively [74–77]. One should be aware, among these four Li-Al phases, two of which exhibit some solubility ranges (dashed lines in figure 3) and these phases can accept/release a certain amount of lithium without altering their crystal structures, i.e. β-LiAl and $Li_{2-x}Al$. For example, a noticeable Li solubility range of β-LiAl is characterized to range from 48.5 at% to 55 at% by melting and mixing Li and Al ingots at 500 °C [78], while the latter yields a smaller solubility range between $Li_{1.92}Al_{1.08}$ (64.0 at%) and Li_2Al (66.7 at%) obtained from the sample that is annealed at 450 °C [73]. The significance of these solubility ranges is rarely discussed in the context of LIBs, which usually operate below 100 °C, perhaps this is because the information of the phase diagram in low temperatures relies on extrapolations of the data obtained at high temperatures [9]. This review will later elaborate (§ 3.3 and § 4.2) on the solubility range of β-LiAl at room temperature and highlight the long-term cycling capabilities of β-LiAl anode as an intercalation material.

2.2. Elevated temperature on the formation of Li-Al alloys in LIBs

Among the Li-Al alloys, β-LiAl is the rightful point to focus on with relevance to the LIB field, since it is the first to form electrochemically at room temperature, while other phases may require elevated temperatures. In a comprehensive study done by Ghavidel *et al,* it is proposed that the electrochemically driven formation of the higher order phases, such as Li_3Al_2 and $Li_{2-x}Al$ phases necessitate working temperatures of at least 35 °C for low rates and 60 °C for moderate rates, and the Li_9Al_4 can only be expected beyond 100 °C [79]. Figure 4 shows some typical galvanostatic profiles from cycling at elevated temperatures with four distinct potential plateaus at 100 °C [79], referring to the four different phases mentioned above, whilst only the first

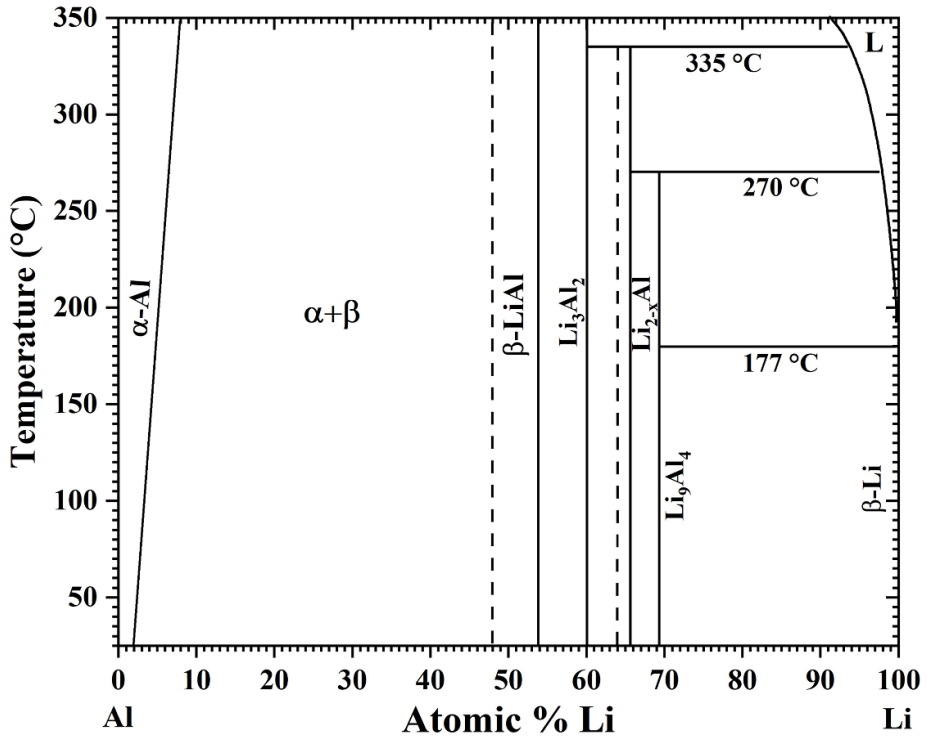

Figure 3. Modified Li-Al binary phase diagram focusing on the temperature regime below 350 °C. The information on all Li-Al intermetallic phases is obtained from the conventional phase diagrams [71, 72], except the $Li_{2-x}Al$ phase that is identified by Puhakainen *et al* in 2010 [73]. The dashed lines indicate the lower boundaries of the solubility ranges [9]. Reprinted from [73], Copyright (2010), with permission from Elsevier.

plateau, i.e. formation of the β-LiAl, can be observed at room temperature. Furthermore, Ghavidel *et al* concluded that by operating at temperatures higher than 35 °C, the specific capacity of Al can nearly double, compared to that of β-LiAl. This two-fold capacity is attributed to $Li_{2-x}Al$ formation and can be achieved by the common operation temperature range of today's commercial cells. As a result, we have drawn a new bar chart that summarizes the capacities of all alloy anode candidates with extra emphasis on Al-based ones to highlight their roles (figure 5). This review will revisit these higher-order phases later in (§ 3.4 and § 4.1), in the context of phase transformation reversibility and cycling characteristics.

2.3. Properties of Li-Al intermetallic compounds

The β-LiAl phase with a cubic structure belongs to the $Fd\bar{3}m$ space group, and is prototypical to NaTl which consists of two distinct diamond sublattices [78]. The lattice parameter of β-LiAl is ~6.37 Å, which is roughly 95% bigger than that of the α-Al (fcc; 4.05 Å) [63]. This volume difference can naturally be expected to cause issues in Al anodes where expansion and capacity are linked. Mechanically, both Li and Al are known to be soft or ductile metals. Yet a ductile-to-brittle transition is observed by transforming Al into β-LiAl [64]. This combination of brittleness and stress gradients likely leads to electrode damage during cycling, as evidenced by cracking, delamination, and pulverization [80, 81]. Kinetically, Li transport in the β-LiAl is several orders of magnitude higher than that in the α-Al [82, 83]. One study even called the β-LiAl 'superionic conductor', underlining the fast diffusion of Li in its lattice [84]. Recently, a new work suggests that this fast diffusion may be a critical factor in determining the ultimate lifetime of β-LiAl phase anodes (§ 6.5) [85]. The ideal stoichiometric composition of β-LiAl is 50:50 in Li:Al ratio and the figure of 993 mAh g^{-1} is calculated directly from this ratio. However, from the old phase diagram, there clearly exists a Li solubility range in β-LiAl (as already mentioned), which is maximized at 520 °C (~11 at%, from 46 at% to 57 at%) [74]. Some studies suggest that this range for β-LiAl would largely be maintained when the temperature is decreased to ambient [86], while others believe it should become significantly narrower, being less than one percent below 100 °C [71]. Since early experiments were done at elevated temperatures, no solid conclusion can be drawn regarding the room temperature solubility (e.g. under electrochemical conditions). A recent study has clarified the electrochemically driven solubility range of the β-LiAl at room temperature and suggested that the range should be roughly 6 at% [9], which is also added to the modified phase diagram in figure 3. Therefore, the fully lithiated β-LiAl (i.e. including the solubility), in fact, holds more Li than the ideal stoichiometry ($Li_{1.000}Al$; 50 at%), yielding a real specific capacity of ~1152 mAh g^{-1}

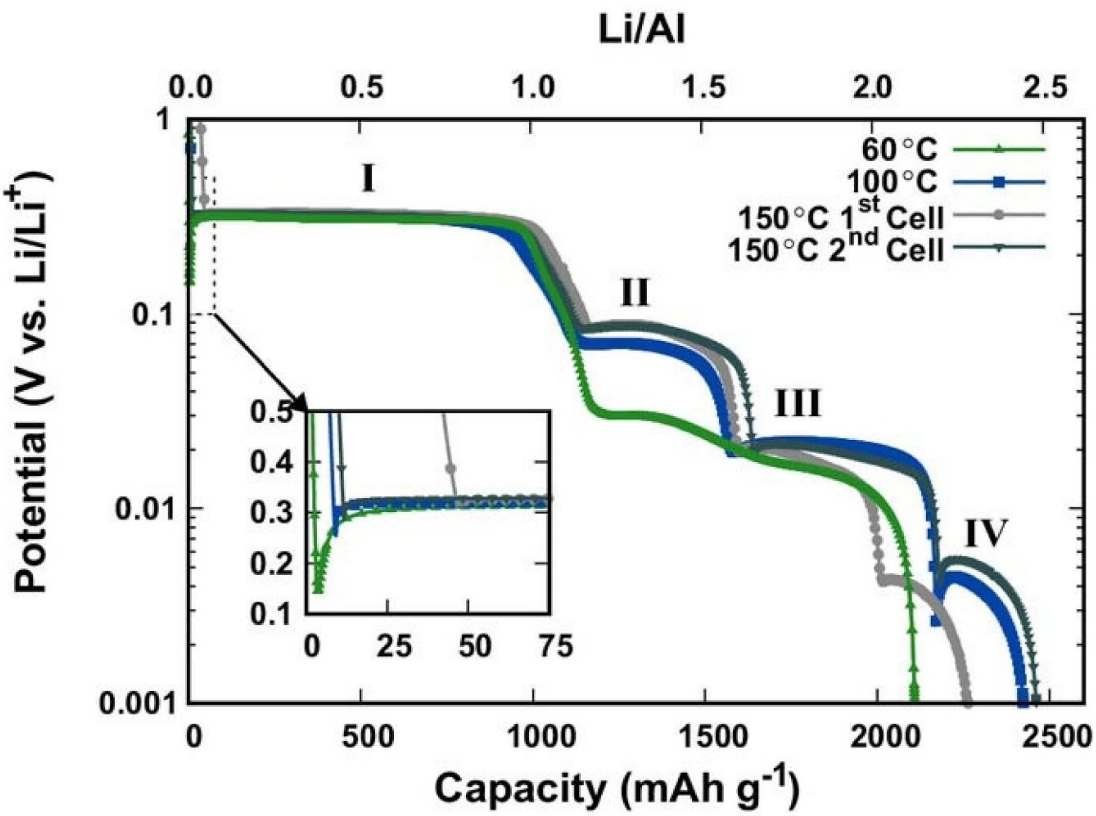

Figure 4. Potential vs. capacity curves for Li-Al cells cycled at three different temperatures. Potentials are shown using a logarithmic scale on the main plot and a linear scale on the inset. Capacities are provided in mAh g^{-1} on the lower axis and as a ratio of Li/Al on the top axis. Plateau regions are indicated with Roman numerals (I–IV). Reproduced from [79]. [© National Research Council Canada and University of Alberta 2019. Published by ECS.]. CC BY-NC-SA 3.0.

($Li_{1.160}Al$; 53.6 at%) [9]. This capacity should also be considered as the theoretical capacity of Al anodes at room temperature instead of the well-adopted 993 mAh g^{-1} in future investigations since the rapid Li transport characteristics of β-LiAl effectively ensure saturation of this phase during lithiation.

Unlike β-LiAl, which started drawing people's attention in the 1970s, the higher-order phases have largely been neglected in the domain of electrochemical energy storage since these phases seem to be only approachable at elevated temperatures ($\geqslant$35 °C for $Li_3Al_2/Li_{2-x}Al$ and $\geqslant$100 °C for Li_9Al_4) as noted previously, or must be synthesized directly [87]. Most literature regarding the phases with a Li content greater than β-LiAl remains in the fields of metallurgy [73] and theoretical calculations [88], e.g. the minima hopping method [89]. In the end, the authors try to summarize available information regarding Li-Al intermetallic compounds in table 1.

3. Electrochemical lithiation of Al

Given the dynamic electrochemical environment of a LIB anode, we next consider specifically how Li gets incorporated into Al from an electrolyte-electrode interface, following a temporal sequence of initial lithiation, nucleation of β-LiAl, α-to-β phase transformation, β phase saturation, and formation of higher order phases (i.e. *true* full lithiation).

3.1. Initial lithiation and nucleation of β-LiAl

Al is known to be a highly reactive metal, and its superior stability under ambient benefits from the passivation Al_2O_3 layer at the scale of several tens of nanometers thick, which is formed as soon as Al is exposed to air. Hence the lithiation of the passivation layer together with the breakdown of electrolyte (i.e. SEI formation) should occur with solid solution lithiation of fcc Al taking place nearly simultaneously. Without a phase transformation, the α-Al can withhold up to approximately 2 at% Li into its crystal structure at room temperature [66]. For practical reasons, overlithiation is likely to occur in many scenarios but is limited due to the extra slow Li diffusion, such that the surface layer of α-Al may reach an upper threshold of ~2.6 at% [94]. Nevertheless, the initial lithiation of Al is usually a rapid process, indicated by

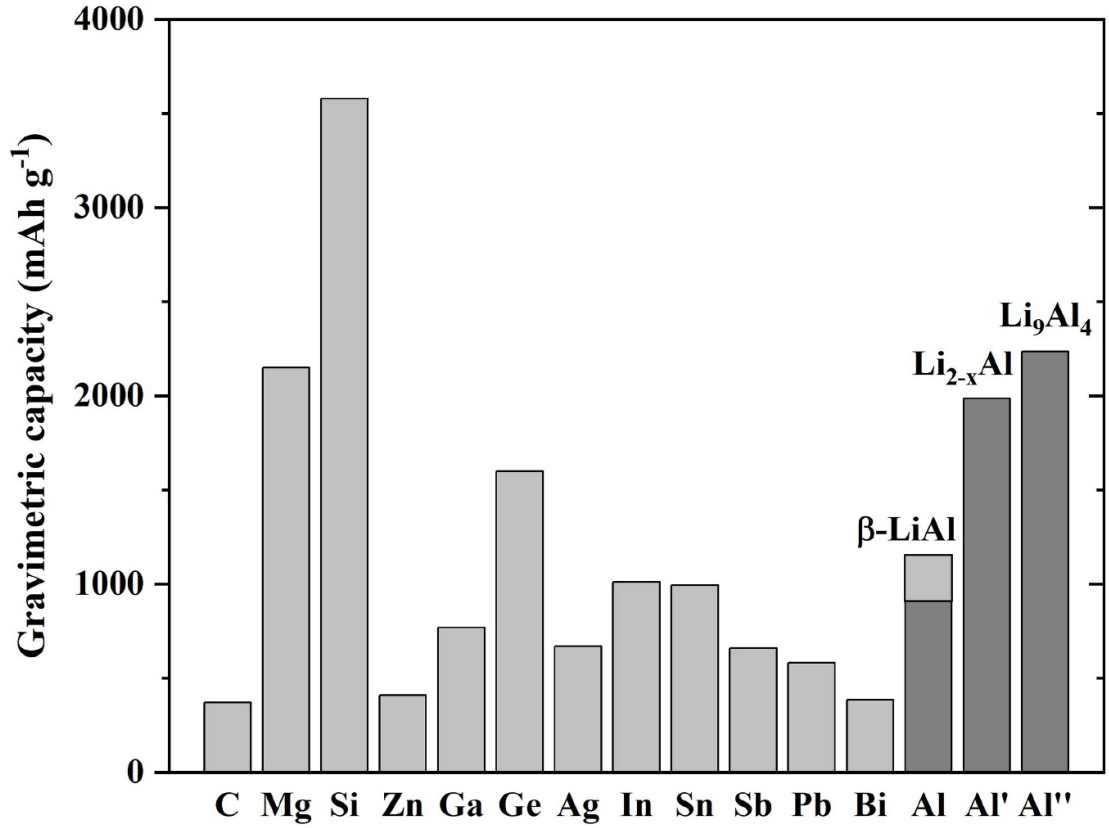

Figure 5. Gravimetric capacities of various alloy anode candidates at the state of full lithiation, with three Li-Al intermetallic compounds specified. The bar of β-LiAl includes its Li solubility range [9]. All data were collected from [36] except the Al ones that are obtained from [79]. Reprinted with permission from [36]. Copyright (2021) American Chemical Society.

Table 1. Properties of Li-Al intermetallic compounds: α-Al, β-LiAl, Li_3Al_2, $Li_{2-x}Al$ and Li_9Al_4. *E, B*, and *G* are Young's, Bulk, and Shear Moduli. The data are obtained from Sarmiento-Pérez *et al* [89], except those that are otherwise stated.

Phase formula	Density (g cm^{-3})	Density (atoms nm^{-3})	Lattice type	*E* (GPa)	*B*/*G* ratio	Lithium diffusivity (cm^2 s^{-1})	Lithium composition (at%)
α-Al	2.7	606	Cubic, face-centered $Fm\bar{3}m$	80.9	2.6; ductile	$\sim10^{-11}$ (RT) [90] $\sim10^{-10}$ (450 °C) [91]	0–2.6 (RT) [90] 0–14.4 (600 °C) [92]
β-LiAl	1.62–1.73 [78]	625–627	Cubic, B32-type $Fd\bar{3}m$	75.7	1.5; brittle	$\sim10^{-8}$ (RT) [93] $\sim10^{-7}$ (RT) [85] $\sim10^{-6}$ (415 °C) [82]	47.8–53.7 (RT) [9] 46.8–55 (415 °C) [82] 48.3–54.5 (500 °C) [78]
Li_3Al_2	1.55	621	Trigonal $R\bar{3}m$	76.4	1.2; brittle	n/a	60 [53]
$Li_{2-x}Al$	1.38 [73]	608	Orthorhombic $Cmcm$	75.4	1.2; brittle	n/a	64[a] [73]
Li_9Al_4	1.27 [73]	596	Monoclinic $C2/m$	59.8	1.3; brittle	n/a	>67 [53]

[a] A small Li solubility is suggested.
n/a: no available data can be found.

the sudden potential drop at the beginning of the galvanostatic profile [95], or the steep decay in current as soon as an overpotential is applied [90].

Nucleation of β-LiAl will proceed after lithium saturation of α-Al (or merely its surface layer), at which time the nuclei are distributed in accordance with numerous factors, including the integrity of interfacial layers, local mechanical compliance, and so forth. From two-dimensional observations, as visualized by

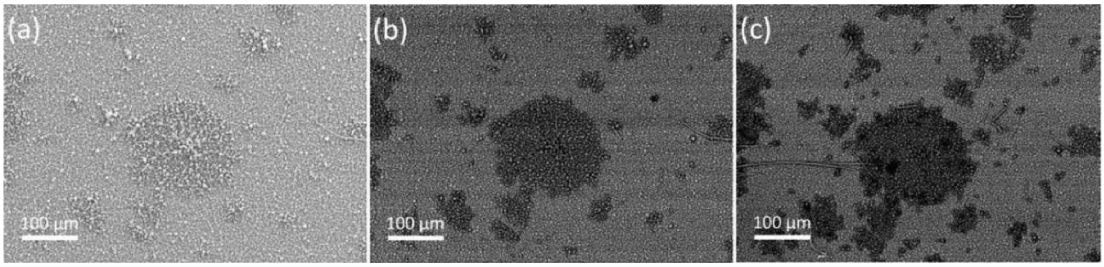

Figure 6. (a) SE and (b) BSE images of the surface of sputtered Al captured after 10 h lithiation; (c) BSE image after 14 h lithiation at a rate of C/20. Reproduced from [80]. [© Tahmasebi *et al* 2018. Published by ECS.]. CC BY-NC-SA 3.0.

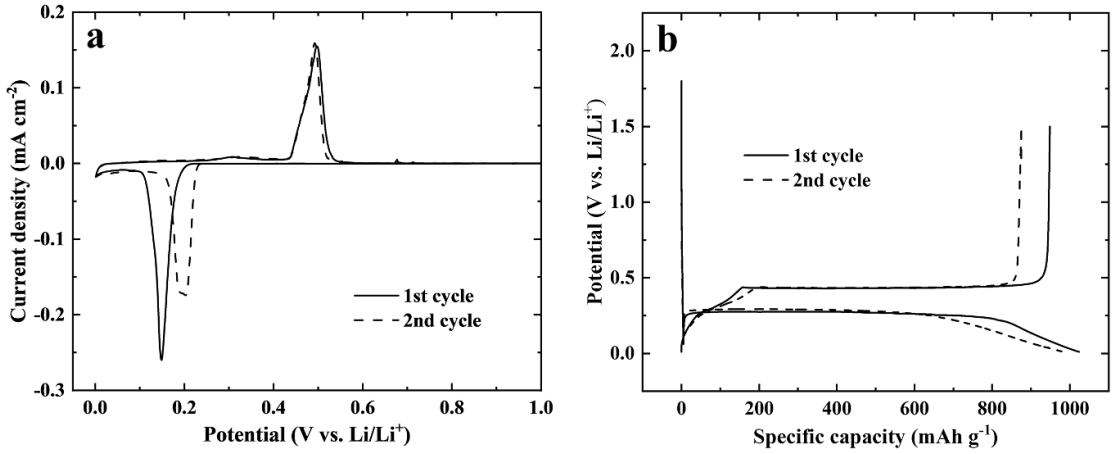

Figure 7. Typical electrochemical profiles for the (de-)lithiation of Al thin films including (a) cyclic voltammograms (CV) and (b) the galvanostatic charge and discharge (GCD) curves. Reprinted with permission from [67] John Wiley & Sons. [© 2020 Wiley-VCH GmbH].

ex situ SEM [80], nuclei have a quasi-circular shape, suggesting some isotropy at the macroscale, although this may not hold true at the atomistic scale, as will be discussed later (§ 3.2.1). Figure 6 shows that the distribution of the β-LiAl patches is indicated by the darker color because of the lower mean atomic number of β-LiAl that scatters fewer electrons as compared to Al under a detector for back-scattered electrons (BSE). The difference in the β-LiAl patch size suggests that some nuclei form before others, which is further affirmed by a series of videos provided by an *operando* light microscopy study (videos S1–S4) [66]. With a sufficient number of growing nuclei, the phase transformation leads to the α-to-β conversion, expansion, and coalescence of the existing β-LiAl patches [96].

Based on classical theory, an energy barrier (e.g. surface free energy) should be overcome to initiate the nucleation of the new phase, as with lithiated compounds in metallic alloys. The first several nuclei should preferentially form at the positions where the energy barrier is minimum, such as grain boundaries and dislocations [97–99]. This extra energy required for the nucleation is electrochemically distinguished by the lower equilibrium potential of the lithiation peak of the 1st cycle in the cyclic voltammogram (figure 7(a)) and the potential dip that is below the plateau at the beginning of lithiation in the typical galvanostatic profile of Al anodes (figure 7(b)). Tahmasebi *et al* suggest that this overpotential might be a result of the mechanical work for deforming the surrounding α-Al [80] (and consistent with later findings [43]), while the grain size and the disorder of Al are also suggested to be responsible [95]. More specifically, Wang *et al* managed to reduce this nucleation energy by alloying Cu with Al since the addition of Cu would decrease the grain size and increase the disordered fraction of the Al (Cu) solid solution. 15 at% Cu is sufficient to reduce the nucleation potential to nearly zero while 20 at% can diminish the extra energy required for the nucleation of β-LiAl [95]. Additionally, it has been found in our preliminary experiments that a carbon coating on an Al foil (e.g. TOYAL-CARBO®) can also effectively reduce this nucleation energy, although further research is needed to confirm why this is the case.

Although the β-LiAl nuclei distribution is seemly random and partly determined by the free energy on the surface of the electrode, the number of nuclei is found to be correlated with the applied potentials. Geronov *et al* proposed two modes of nucleation: instantaneous and progressive [96]. When an Al electrode is held at a certain potential below equilibrium vs. Li/Li$^+$, a fixed number of β-LiAl nuclei should form

instantaneously, which grow and merge until the end of the lithiation. However, if the applied potential jumps to lower levels (i.e. higher overpotentials), additional nuclei are expected, referring to progressive nucleation. Later both modes were visually revealed under a light microscope [66]. In short, a low potential vs. Li/Li^+ leads to more β-LiAl nuclei in either mode. For most planar geometries (e.g. films and foils), the nuclei will coalesce within the first Z nm of electrode thickness/depth from the electrolyte interface.

3.2. α-to-β phase transformation (plateau; lithiation)

After initial lithiation and nucleation, the Al electrode enters a stable stage of phase transformation. The coexistence of the two phases yields a sharp lithiation peak in the cyclic voltammogram in figure 7(a) and a flat lithiation plateau in the galvanostatic profile in figure 7(b), respectively, indicating the phase transition from α-Al to β-LiAl. The growth mechanisms of the β-LiAl may vary with different electrode designs, so thick foils, thin films, and composites are discussed here.

3.2.1. Lithiation kinetics and mechanisms

For **thick Al foils**, the β-LiAl nuclei initially form at the interface between the electrode and the electrolyte. These nuclei grow 3-dimensionally (3D), and merge with each other, quickly covering the whole surface of the Al foil. Afterward, 1D growth along the *Z*-axis must take place until the end of the phase transformation. This 1D growth mechanism is often described by the empirical Deal–Grove model (i.e. surface oxidation of silicon), which are suitable for modeling the lithiation process of various materials when the movement of the interface is reaction- or diffusion-controlled [100, 101]. Conveniently, oxygen diffusion in the oxide layer of silicon can be considered equivalent to the Li diffusion in the β-LiAl layer [102]. Therefore, the Li diffusivity together with the overall thickness of the Al foil that is being lithiated (i.e. diffusion distance) determines whether the lithiation process is reaction-limited or diffusion-limited. Thanks to the fast Li diffusion in β-LiAl, lithiation of Al in most cases is limited by the chemical reactions at the phase front between the α and the β phase [82, 90]. Table 1 also highlights that the Li diffusivity in β-LiAl is roughly three orders of magnitude higher than that in α-Al.

In the case of **Al thin films** being deposited on a substrate, the initial growth of nuclei will still be 3D. However, the finite thickness can largely limit the in-depth growth as soon as the β-LiAl hits the substrate. Therefore, a shift from 3D to 2D growth must occur, at which the individual nuclei can impinge with each other. Then each nucleus expands laterally following a quasi-circular shape and starts merging with others until the end of lithiation. The whole process was visualized by a series of videos made by a light microscope (videos S1–S4) [66, 67]. It should be mentioned that the Deal–Grove is no longer valid in this case. Instead, Avrami equations are the appropriate tool to model the lithiation of Al films [103–105]. A kinetic study of lithiation of Al thin films suggests that this 2D growth of the β-LiAl is also a reaction-limited process [66]. In addition, this 2D expansion is likely affected by the orientations of the surrounding Al grains. The <111> out-of-plane orientation with densely packed Al atoms is found to be more reluctant to lithiation than other textures [65].

Lastly, several studies are working on **Al composite electrodes** following the slurry-based fabrication approach [106–108]. The lithiation of composite Al powder is different, where a circular particle is used as the model system. A comprehensive study has schematically illustrated the whole lithiation process of Al particles (figure 8), in which the reaction-limited process at the phase boundary is also highlighted. Interestingly, this study has also introduced the relevancy of Li-rich (i.e. beyond the β-LiAl) amorphous phases at the end of lithiation [109], which will be discussed later.

3.2.2. Mechanical effects

Owing to the volume expansion caused by lithium incorporation, significant stresses are often associated with almost all alloy anodes, such as silicon and germanium, which will give a nominal compressive stress of >1 GPa upon full lithiation [110, 111]. This level of stress can cause certain mechanical issues, thereby significantly affecting the electrode integrity and its electrochemical performances [52].

The mechanical effects of Al are discussed here using **Al thin films** as the model system. The substrate curvature method is applied in a recent study that has quantified the nominal stress (thickness change is not considered) of an Al thin film electrode deposited on a substrate [67]. It can be seen from figure 9(a) that a compressive stress of ~500 MPa is generated upon a complete α-to-β transformation. Although the stress level is lower than that of Si/Ge electrodes mentioned above, it is still high enough to cause cracking and delamination of the Al thin film electrode, which are also observed under a light microscope [66, 67], as well as an electron microscope [81]. Importantly, one can find that an almost linear buildup of compressive stress is observed in accordance with a constant current and the corresponding conversion at a constant rate. The random nucleation and 2D growth of the β-LiAl for Al thin films, which gives the linear change of the phase fractions of α and β, should largely explain this buildup of the compressive stress [66, 67]. It should be

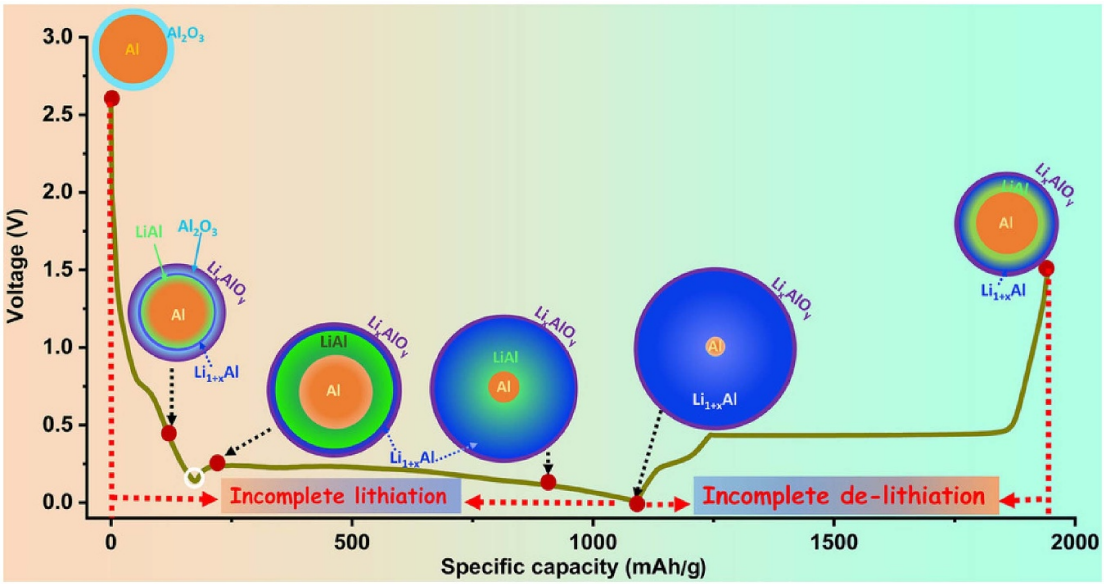

Figure 8. Schematic illustration of the first cycle of the lithiation/delithiation process of an Al anode. Reprinted with permission from [109] John Wiley & Sons. [© 2019 Wiley-VCH Verlag GmbH & Co. KGaA, Weinheim].

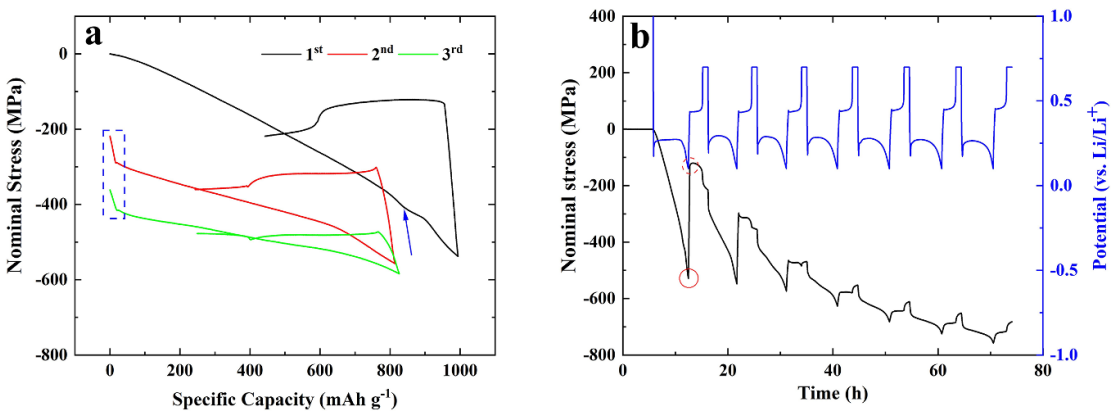

Figure 9. (a) Nominal stress as a function of specific capacity obtained from an Al thin film electrode: data of the first three cycles are plotted: black (1st), red (2nd), and green (3rd cycle). (b) Nominal stress as a function of time coupled with the potential response for the whole experimental process. Reprinted with permission from [67] John Wiley & Sons. [© 2020 Wiley-VCH GmbH].

acknowledged that this seemly linear behavior of compressive stress is also different from Si and Ge, which yield a rapid stress increase at the beginning of lithiation (quasi-elastic; interstitial sites) and then followed by a stable stress response (quasi-plastic; yielding point) [52, 111–113]. At the later stage of lithiation that is indicated by the blue arrow, a stress kink is observed, suggesting a likely different mechanism of the compressive stress accumulation. This will be elaborated together with the Li solubility range of β-LiAl (§ 3.3 and § 4.2). Additionally, an interesting feature of continuous stress accumulation over cycling is observed in figure 9(b). This observation suggests that the lithiation-delithiation of the Al film electrode is not fully reversible, which will also be discussed in detail later (§ 5.1).

Despite generating insightful results with Al thin films, the substrate curvature method is ill-suited for monolithic **Al foils**. In fact, the stress behavior of an Al foil is more complicated due to the in-depth lithiation. The initial nucleation and growth of the β-LiAl should replicate that of a thin film. When the surface of an Al foil is fully covered with the β-LiAl, the growth via the Z-axis should take over and dominate the lithiation process. This in-depth phase transition of a partly lithiated Al foil is visualized by SEM images. Again, a BSE detector is used to distinguish the two phases with different mean atomic masses. Figures 10(a) and (b) presents the cross-sectional views with and without a tilting angle at two magnifications, where a rough and corrugated phase interface is observed, which is likely a result of the random nucleation and initial 3D growth [66, 96]. Although the overall phase transition should follow a 1D growth mode, inhomogeneities

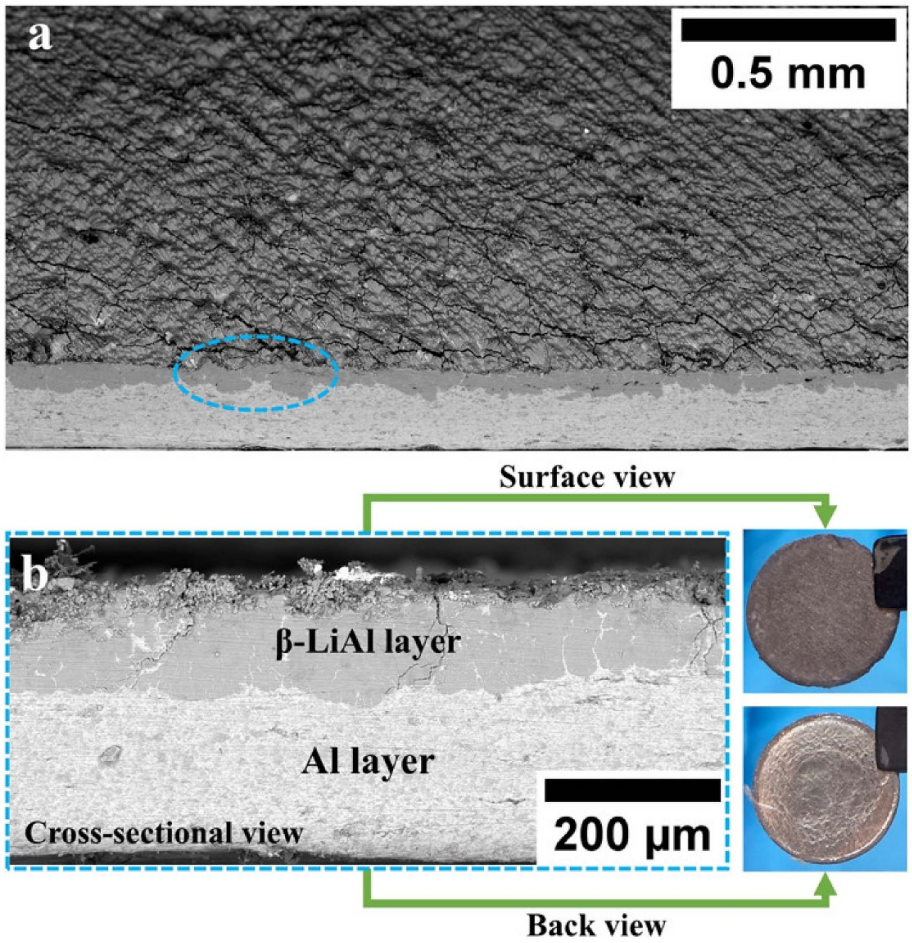

Figure 10. (a) SEM image taken for a partially lithiated Al foil using a 90° sample holder with a tilting angle of 45°, of which the crosssection is enlarged in (b) at a magnitude of 200×. The macroscopic views of the electrode surface and the backside are also shown. Reproduced from [9]. CC BY 4.0.

may lead to variations in phase evolution. Yet the overall structural integrity of the Al foil electrode seems to be properly maintained, as can be seen in the photographic images.

3.2.3. Structural changes

On the lithiation plateau, the β-LiAl patches keep growing, causing a continued increase of mechanical stress, which can plastically deform the surrounding α-Al grains. This mechanical deformation can lead to the formation of dislocations and smaller grains [63, 65, 67]. Overall, the structural changes during lithiation are schematically summarized in figure 11. When an Al thin film is being lithiated, ∼95% volume expansion is inevitable due to the Li inclusion (figures 11(a) and (b)). As mentioned, the internal stress drives the grains to deform and become very small (figure 11(c)). After a complete cycle, an Al thin film electrode with finer grains is generated. The Al grains size is found to decrease from ∼100 nm to ∼5–10 nm after repeated lithiation–delithiation cycling (figure 11(d)) [63]. Despite the graphene coating on the electrode surface, the illustrated microstructure evolution is believed to be representative of Al anodes, which can also be supported by other studies [67, 68].

3.3. Completion of β phase formation (non-plateau; lithiation)

One can notice that the lithiation plateau in the galvanostatic charge and discharge curves no longer exists at the end of lithiation, regardless of the electrode architecture, e.g. Al films (figure 7) and Al composites (figure 8), or even Al foils in [36]. This regime of the last ∼20% of the lithiation has been rarely discussed in the literature, and with some inconsistencies when it is mentioned. Various explanations can be found in the existing literature, such as Li solubility of β-LiAl [9], amorphous $Li_{1+x}Al$ phases [109], and $Li_3Al_2/Li_{2-x}Al/Li_9Al_4$ phases [60, 63].

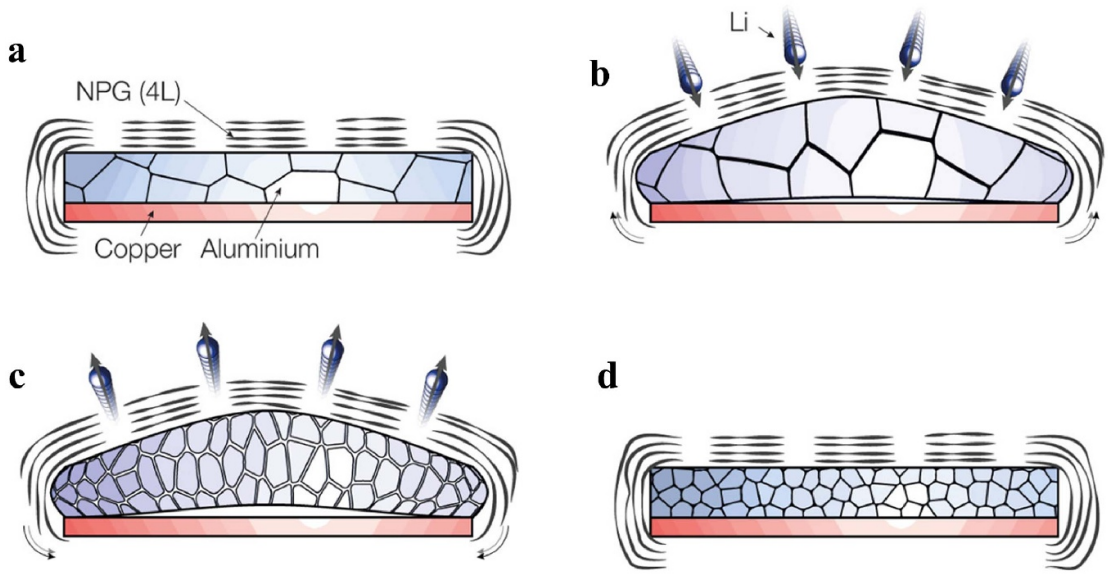

Figure 11. Schematics summarizing the lithiation−delithiation cycle of a graphene-coated Al thin film anode: (a) pristine electrode, (b) lithiation process, (c) delithiation process, and (d) delithiated electrode. Reprinted with permission from [63]. Copyright (2018) American Chemical Society.

3.3.1. Saturation of β-LiAl

Although there is almost no question that β-LiAl exhibits a solubility range at elevated temperatures, the inconsistency comes from the lower temperature regime. As evidenced by multiple versions of the Li-Al phase diagrams, different extrapolations to room temperature have been suggested, ranging from less than one percent (ca. 49.2–50.1 at% Li) [74] to a solubility range of 9.2 at% Li [114]. Recently, a study is conducted specifically on characterizing the solubility range of β-LiAl at room temperature, determining a ~6 at% range of Li solubility within β-LiAl (figure 3). As shown in figure 12, this solubility range can yield ~242 mAh g^{-1} specific capacity, normalized to Al, which is suggested to be largely correlated with the non-plateau regime [9]. When the electrode contains a single phase, i.e. β-LiAl, its potential would decrease with additional Li inclusion, rather than stay at the plateau of α/β coexistence.

3.3.2. Mechanical effects

Apart from electrochemistry, this non-plateau regime also gives rise to a different path of mechanical evolution. As mentioned above, in figure 9, a kink in the stress signal appears when the potential plateau approaches its end, after which the growth of compressive stress seems to show a higher slope against time. The origin of this faster stress growth at the end of lithiation is still unclear. One explanation may be that it is a result of saturating the solubility range within the β-LiAl as the overall volume change may strain the substrate more significantly than the two-phase coexistence where the stress is restricted at the phase interface [9, 67]. This is complicated by the facts that the hardness (figure 13(a)) and yield strength (figure 13(b)) of β-LiAl are known to vary markedly across its composition range, but also that significant defect generation and work hardening occur in the residual α-Al matrix [43, 67]. More information and discussion will be provided in § 5.1.

3.3.3. Formation of amorphous $Li_{1+x}Al$ phases

It is still questionable whether the formation of Li-rich phases (i.e. Li content higher than β-LiAl) is occurring at room temperatures. Although these phases are only supposed to exist at elevated temperatures, they are mentioned from time to time in the literature. For instance, both Li_3Al_2 and Li_9Al_4 peaks seem to appear in the x-ray diffractograms obtained *ex situ* [60]. Another study claims that Li_3Al_2 is detected from a lithiated Al film, in addition to β-LiAl [63]. Yet some other studies claim that Li-rich phases can hardly form at room temperatures [79, 80]. Regarding these inconsistencies, Li *et al* have commented that these Li-rich phases may be formed, but are only limited to a very thin layer on the electrode surface and the overall equilibrium is still α/β [43].

Apart from mentioned above, a study of **Al composite electrode** (figure 8) proposes a very different mechanism for lithiation [109], especially for the end of lithiation (non-plateau). An *in situ* x-ray diffraction (XRD) test was done neatly in the same study, providing a series of diffractograms covering the whole

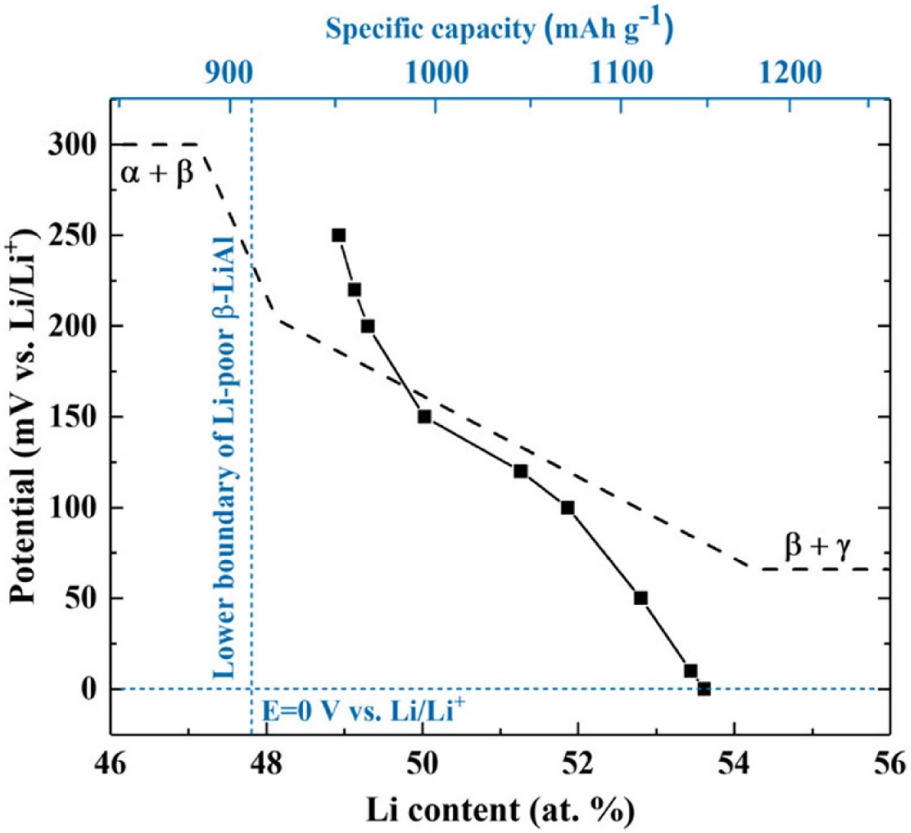

Figure 12. Potentiostatic charge counting data obtained from 0.25 mm-thick Al foils (99.997% purity) covering a potential range from 250 to 0 mV versus Li/Li$^+$ at room temperature, with the possible lower limit of the solubility range specified. Reproduced from [9]. CC BY 4.0.

lithiation–delithiation processes (figure 14(a)). At the first glance, the XRD peaks of crystalline Al show reasonable trends with high intensities at the beginning of lithiation and the end of delithiation. The minimum is observed at the end of lithiation where all Al is consumed. Differently, the <111> LiAl peak exhibits a noteworthy behavior: Its intensity in the diffractograms reaches the highest at the end of the lithiation plateau (i.e. ∼80% of the lithiation), and then sharply drops to nearly zero when lithiation finishes. The <220> LiAl peak gives a similar trend, but its intensity decreases more gently and is non-zero at the end of lithiation. It becomes obvious when the peak intensities are extracted and plotted in figure 14(b). Based on these observations, it is interpreted that over-lithiated phases are forming at the expense of the β-LiAl during this regime. Since the β-LiAl and Al peaks are the only ones that are detectable under x-ray, these over-lithiated phases are generalized to be $Li_{1+x}Al$ and suggested to be amorphous [109], but likely such trends are restricted to particle-based Al anode materials.

3.4. Formation of Li-rich phases (extra plateaus; lithiation)

Different from the amorphous $Li_{1+x}Al$ phases proposed by Qin *et al* that may occur at room temperature [109], this section focuses on the Li-rich phases (i.e. Li content higher than β-LiAl) that are present in the modified Li-Al binary phase diagram (figure 3) that are expected to be approachable at elevated temperatures. As already mentioned, unlike the β-LiAl, only a few studies have investigated these higher-order phases electrochemically.

3.4.1. Formation of Li_3Al_2, $Li_{2-x}Al$, and Li_9Al_4

Ghavidel *et al* have conducted *ex situ* XRD experiments to obtain the diffractograms of the lithiated Al foils at various temperatures. As can be seen from the bottom of figure 15, there are only diffraction peaks of crystalline β-LiAl with two weak residual α-Al peaks marked at 30 °C. At elevated temperatures, the diffractograms generally contain peaks of two Li-Al phases. For instance, the diffraction peaks of both Li_3Al_2 and $Li_{2-x}Al$ are observed at 60 °C based on JCPDS cards 26–1008 (Li_3Al_2) and 1–79-8685 ($Li_{2-x}Al$). Similarly, for the Al foils that are lithiated at 100 °C and 150 °C, peaks of both $Li_{2-x}Al$ and Li_9Al_4 (JCPDS 24–0089) are observed. By coupling the *ex situ* XRD with systematic electrochemical tests, it is concluded that the Li_3Al_2 and $Li_{2-x}Al$ can form at a very slow (e.g. ∼C/120) and at a moderate (e.g. ∼C/30; considering

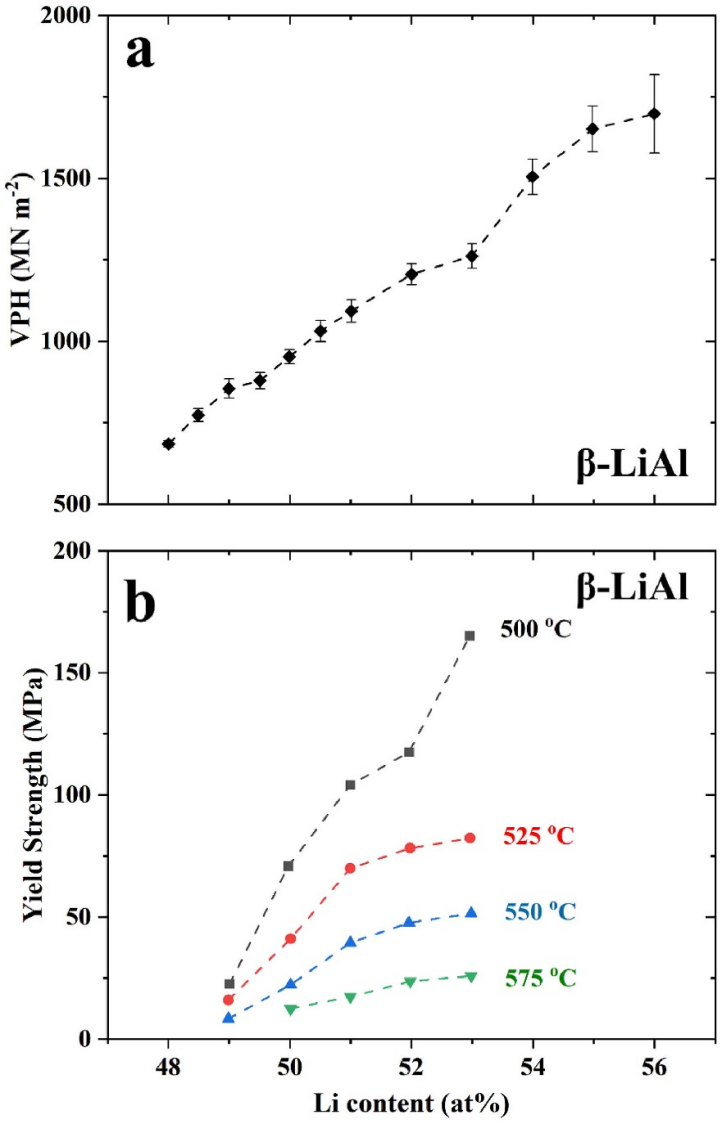

Figure 13. (a) Variation of the hardness of β-LiAl with the compositions measured at room temperature. (b) Variation in the yield strength of β-LiAl with the composition at different temperatures. Data are obtained from [64, 115]. Reprinted from [64], Copyright (1987), with permission from Elsevier.

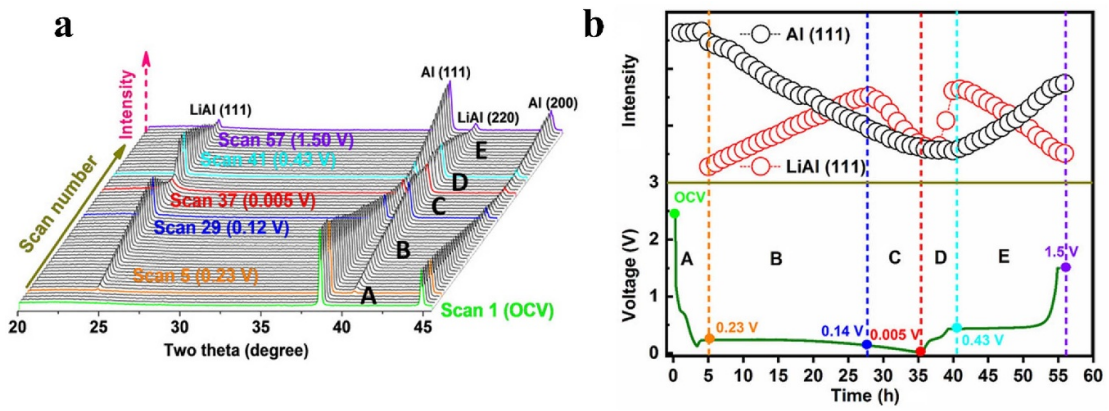

Figure 14. (a) *In situ* XRD of the Al electrode upon the first cycle and (b) corresponding (de-)lithiation profiles together with the XRD intensity variation for the Al <111> and LiAl <111> reflections (electrolyte:1 M $LiPF_6$–EC/DMC, volumetric ratio:1:1). Reprinted with permission from [109]. John Wiley & Sons. [© 2019 Wiley-VCH Verlag GmbH & Co. KGaA, Weinheim].

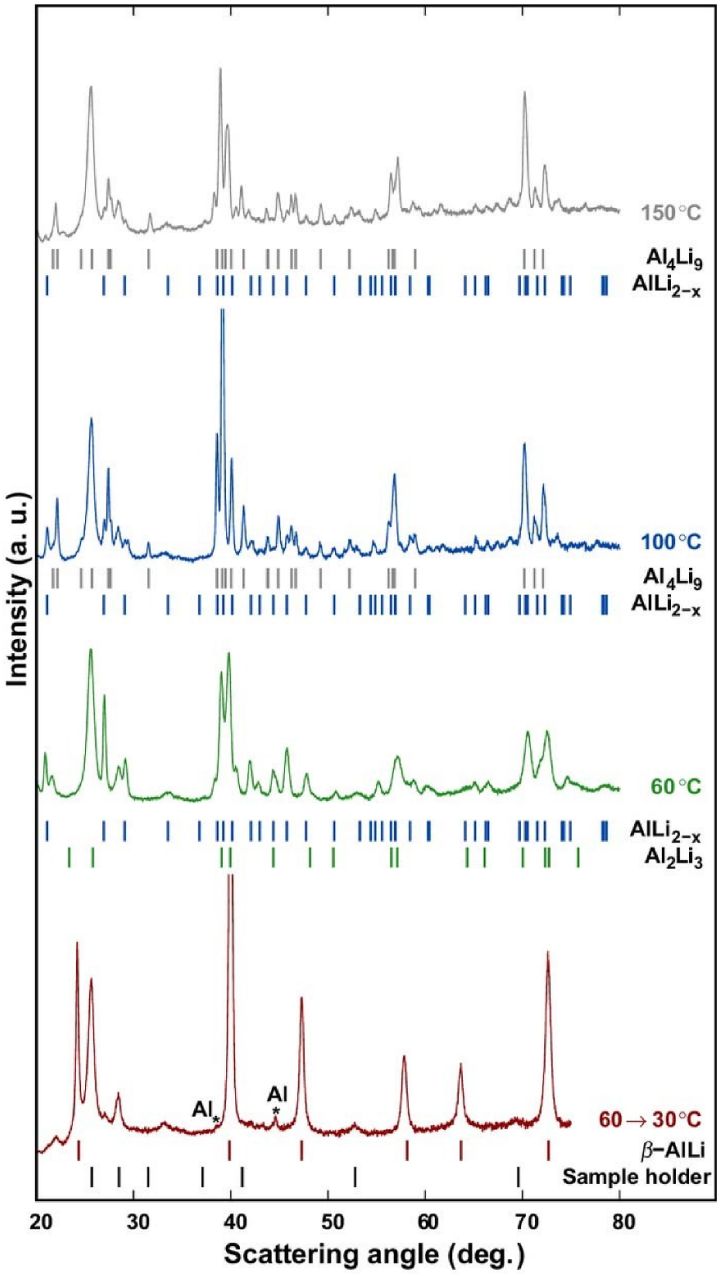

Figure 15. X-ray diffractograms collected from Al foils (13 μm thick; 99% purity) that are lithiated to 0.001 V vs. Li/Li$^+$ at different temperatures. The diffractogram obtained at 60 $\rightarrow$ 30 °C is from the Al foil that undergoes a complete cycle at 60 °C and is then lithiated at 30 °C. Peak positions from reference patterns and the sample holder are indicated. Reproduced from [79]. [© National Research Council Canada and University of Alberta 2019. Published by ECS.]. CC BY-NC-SA 3.0.

β-LiAl capacity) lithiation rate, when the temperature is above 35 °C and 60 °C, respectively. The formation of Li_9Al_4, on the other hand, requires a temperature above 100 °C. It is also suggested that the formation of Li_3Al_2 and $Li_{2-x}Al$ appears to be linked while Li_9Al_4 seems to be governed by a different formation mechanism [79].

3.4.2. Opportunity for moderate temperatures

In our daily lives, almost everyone has experienced their smartphones or other portable electronics to heat up during active use and charging. Indeed, even with ambient temperatures of 26 $\pm$ 0.5 °C, smartphones can easily reach beyond 43 °C from app usage alone [116]. Considering larger-scale applications of LIBs, such as EVs and stationary energy storage, overheating of the battery pack could be more problematic, leading to drastic incidents like fire catching or even explosion. The situation explains why the sophisticated cooling system is the key component for commercial EVs. Of course, high temperatures, e.g. >100 °C, are beyond the stability of LIB electrolytes, but operating LIBs at slightly elevated temperatures is acceptable or even preferred due to a faster ion diffusion. A commonly acceptable temperature range, as mentioned in the data

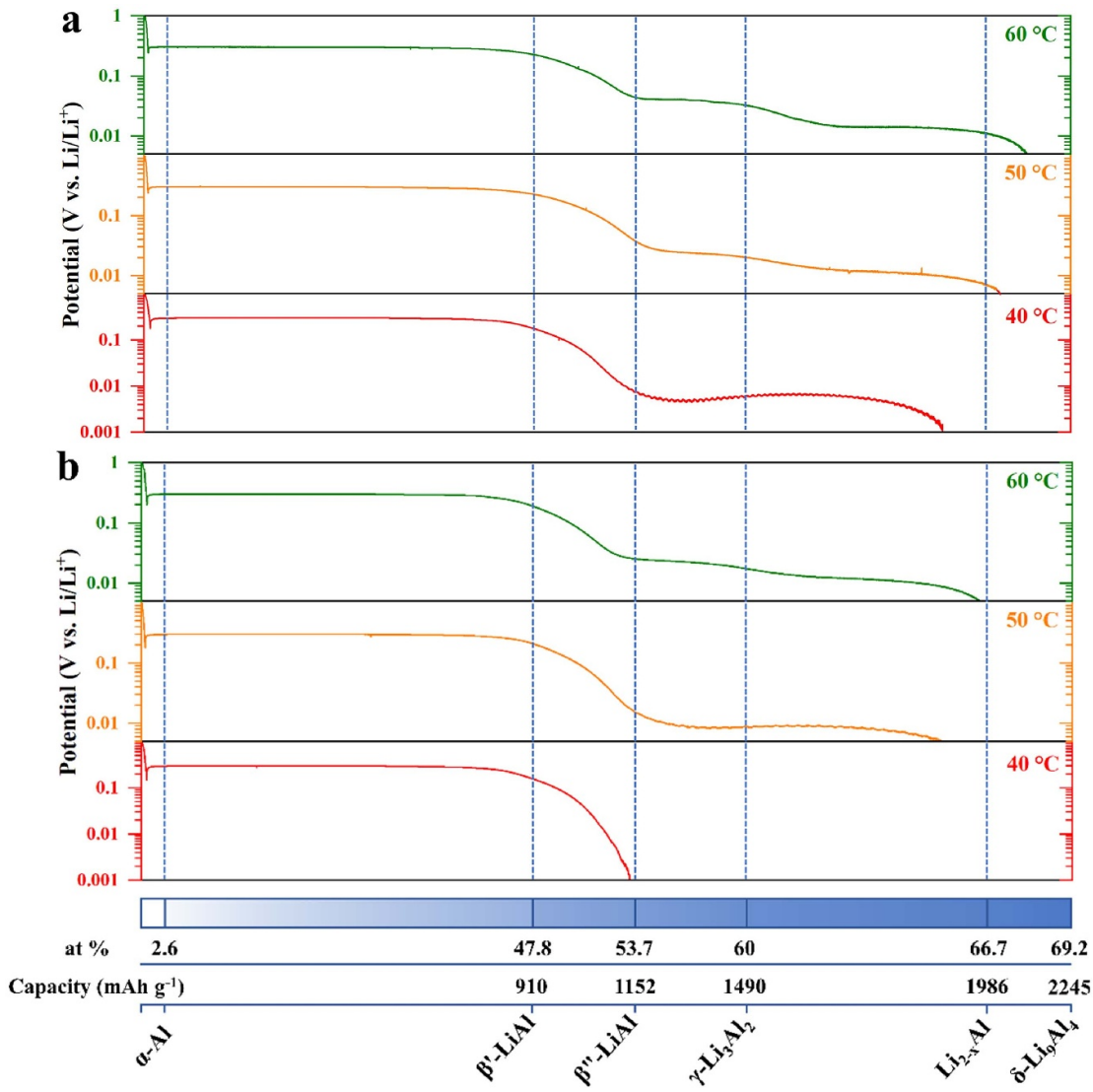

Figure 16. Electrochemical lithiation of Al thin film (∼1.8 μm) electrode on Cu foil substrate at various temperatures within the moderate temperature regime. The lithiation current under galvanostatic mode is (a) 24 μA cm^{-2} and (b) 48 μA cm^{-2}, which are equivalent to ∼C/20 and ∼C/10, respectively, normalized to the theoretical capacity of the β-LiAl. Reproduced from [118] CC BY 4.0.

sheets of many commercial LIB products, is naturally limited to moderate levels (⩽60 °C) to ensure safe and reliable operations [117].

Recently, one study only focuses on the moderate temperature regime and compares the Al thin films that are lithiated at different rates and temperatures. With a small lithiation current of 24 μA cm^{-2} (figure 16(a)), the three plateaus referring to the formation of β-LiAl, Li_3Al_2, and $Li_{2-x}Al$ can be clearly observed at 60 °C and 50 °C with the y-axis in a logarithmic scale. However, when the temperature is further decreased to 40 °C, the second (Li_3Al_2) and the third plateau ($Li_{2-x}Al$) seem to merge with each other, yielding a long plateau until reaching a specific capacity level that roughly matches the $Li_{2-x}Al$ one. At 40 °C, when the Al film has been transformed to the β-LiAl (i.e. >47.8 at% Li or >910 mAh g^{-1} Al), the lithiation potential drops to a level as low as ∼4 mV vs. Li/Li$^+$ and slowly recovers to ∼7 mV vs Li/Li$^+$. This potential level is sufficiently low (i.e. <15 mV vs. Li/Li$^+$) to facilitate the simultaneous formation of Li_3Al_2 and the $Li_{2-x}Al$. This experiment is also repeated at a higher lithiation current of 48 μA cm^{-2} and the results are shown in figure 16(b). Although the galvanostatic profile at 60 °C almost maintains the same features, the potential plateaus of the Li_3Al_2 and the $Li_{2-x}Al$ start merging at 50 °C under this higher rate rather than at 40 °C under the lower rate. Remarkably, the phases that are beyond β-LiAl can hardly form at 40 °C and the lithiation effectively stops with the β-LiAl composition [118].

In the end, what enables Al to reach its full capacity (figure 1) at room temperature is unclear. Certainly, diffusion limitations in the highly ordered Li-Al phases must be considered, but as evidenced by the initial $\alpha \rightarrow \beta$ phase transformation, nucleation barriers/potentials can also be expected to play a role. Therefore,

the purity of Al (or amount and type of impurities, rather) may have a very big impact on the ability to realize the phases with the highest capacities. This should be anticipated as a very exciting area for research, not just because of the theoretical merits, but also because of the practical implications for the world's most produced base metal [119, 120].

4. Electrochemical delithiation of Li-Al alloys

In this chapter, the reverse phase transformations, i.e. Li extracted from Li-Al alloys electrochemically, are elaborated. The delithiation is presented in different ways depending on whether the fully lithiated phase is Li_9Al_4, $Li_{2-x}Al/Li_3Al_2$, or β-LiAl, with discussions following the trend of the most lithiated, to the least.

4.1. Delithiation and cycling of Li-rich phases (extra plateaus; delithiation)

Owing to their difficulty in the formation of Li_3Al_2, $Li_{2-x}Al$, and Li_9Al_4, knowledge about the delithiation pathway from higher-order Li-Al phases to lower-order ones is rather limited. Nevertheless, the extremely low standard potential of Li_9Al_4, relative to Li/Li^+, should make reversible cycling a challenge. Indeed, as noted by Kim *et al* [87], 'It is apparent that Li tends to deposit and grow around Li_9Al_4'. So, while from a gravimetric/volumetric capacity perspective, such a phase is probably interesting for primary battery applications, the reversibility of the phase transformations poses a long-term challenge for secondary lithium-ion cells. The Li_3Al_2 and $Li_{2-x}Al$ phases, on the other hand, offer excellent capacities but should allow for delithiation and reversibility, at least at elevated temperatures as the delithiation of $Li_{2-x}Al$ and Li_3Al_2 corresponds to 0.04–0.05 V vs. Li/Li^+ for the former and 0.1–0.2 V vs. Li/Li^+ for the latter. As noted in § 3.4, the extent of thermal energy required to form these phases may only be slightly above room temperature, but this leads to the natural question: Can these phases be cycled reversibly?

Recently, a new cycling approach is proposed to cycle the Al electrode at moderate temperatures, which does not trigger the formation of Li_9Al_4 while the $\alpha \leftrightarrow \beta$ phase transformations are also intentionally prohibited. As a result, as shown in figure 17(a), the electrode is only cycled between β-LiAl and $Li_{2-x}Al$ by controlling the temperature and restricting the potential window. Since the phase transformations involved in this new cycling approach are different from the well-studied $\alpha \leftrightarrow \beta$ ones, the cycling behavior is expected to be also different due to different material properties. The outcome turned out to indeed be true, that the cyclability of β-LiAl $\leftrightarrow$ $Li_{2-x}Al$ is significantly better than that of $\alpha \leftrightarrow \beta$ (figure 17(b)) [118]. Not only does this finding open up opportunities in real applications as the heat generated by ohmic resistance must be dissipated during operation, but also provides new topics to researchers who are interested in Al-based anodes that have greatly improved stability (β-LiAl $\leftrightarrow$ $Li_{2-x}Al$ cycling) and capacity (1986 mAh g^{-1} Al for $Li_{2-x}Al$).

4.2. Delithiation of β-LiAl (non-plateau; delithiation)

As β-LiAl is often considered the fully lithiated phase in the LIB field, we return to this section by focusing on the delithiation of β-LiAl at room temperature. Two scenarios of delithiation are discussed: (1) the desaturation of β-LiAl (non-plateau) in this section and (2) the β-to-α phase transformation (plateau) in the next.

Assuming the β-LiAl is the only relevant phase present, the initial delithiation begins with a depletion of the Li while maintaining the crystal structure of β-LiAl [9]. Electrochemically, this desaturation is indicated by the potential increase at the beginning of delithiation, occupying roughly 20% of the β-LiAl capacity prior to the delithiation plateau (figure 7(b)). This number is generally in agreement with the one characterized by the charging counting method in figure 12, i.e. 242 mAh g^{-1}-Al. It is still uncertain whether the Li concentration is homogeneous over the whole electrode. Therefore, the desaturation process is possibly location-dependent, e.g. some parts of the electrode may be desaturated prior to others. However, given the good diffusivity of Li in β-LiAl, homogeneity may be expected. When the Li concentration within the β-LiAl approaches its minimum (e.g. 47.8 at%) [9], the nucleation of, and reversion to, α-Al must occur.

The solubility range shifts the lattice parameter of the β-LiAl unit cell, as Li atoms are being inserted/extracted while maintaining the same crystal structure. The shift in lattice parameter as a function of the Li content within β-LiAl was studied and summarized in table 2 [78]. As can be seen, the lattice parameter of the cubic β-LiAl unit cell ranges from ~6.3902 Å to ~6.3612 Å when the Li-rich β-LiAl is desaturating to form the Li-poor β-LiAl. Also, insertion/extraction of Li from β-LiAl varies the density, giving >0.1 g cm^{-3} difference between the Li-rich and the Li-poor β-LiAl. A corresponding asymmetrical mechanical evolution of the electrode is observed during the desaturation of β-LiAl (figure 9(a)). One can notice that a sudden increase of the stress towards the tensile direction is observed as soon as the current direction is reverted. This is an indication of the overall volume contraction of ca. 1.4% within a single phase, as noted above, that strains the substrate drastically, causing this substantial stress change. After the

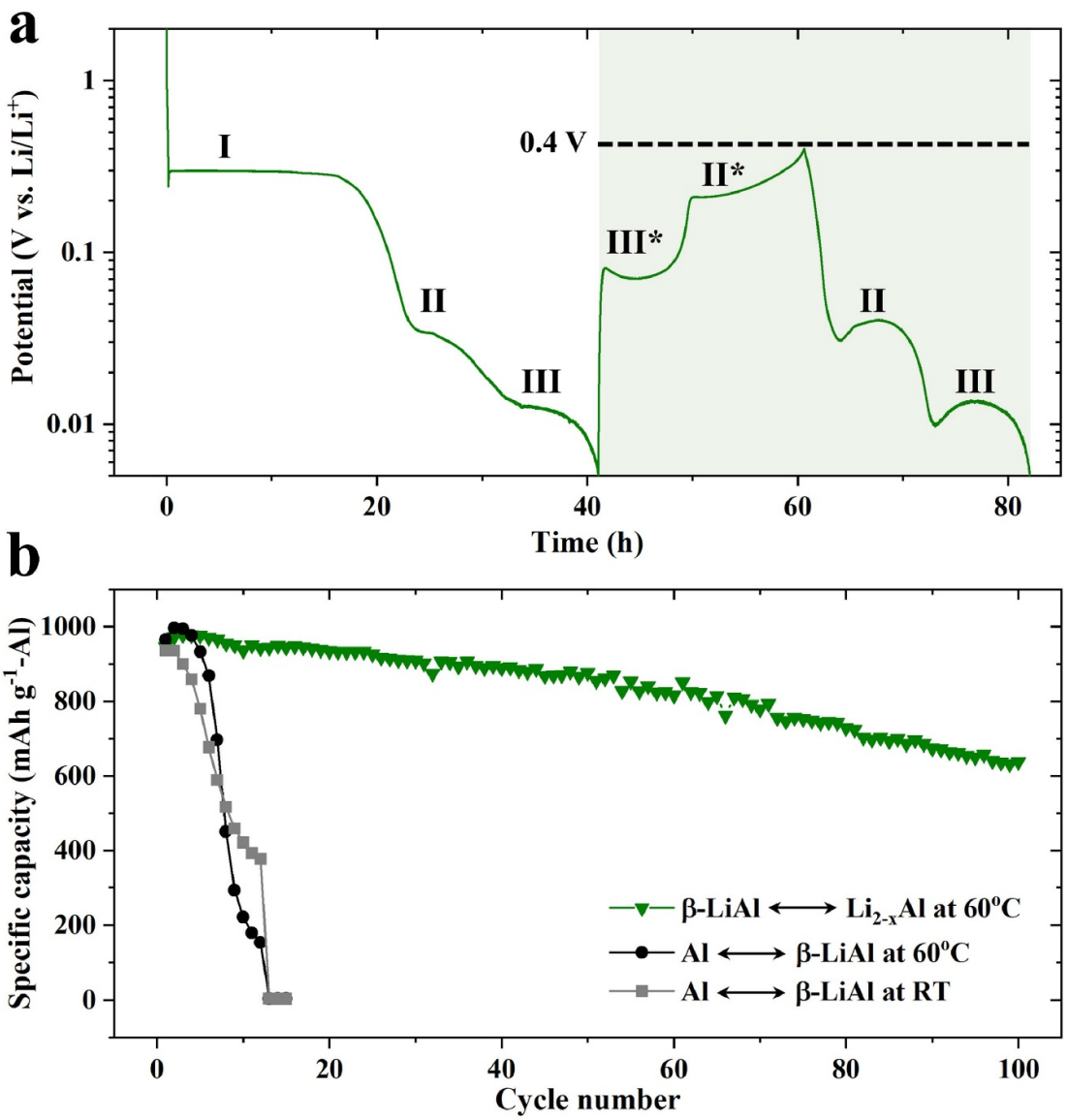

Figure 17. (a) An alternative of galvanostatic cycling that utilizes the capacity contributed by β-LiAl $\leftrightarrow$ $Li_3Al_2 \leftrightarrow Li_{2-x}Al$ phase transformations ($\alpha \leftrightarrow \beta$ phase transformations are prohibited); (b) the cycling performance of the β-LiAl $\leftrightarrow$ $Li_3Al_2 \leftrightarrow Li_{2-x}Al$ phase transformations, i.e. between III*/II* and II/III in (a), which is compared with the ones of the $\alpha \leftrightarrow \beta$ phase transformations. Reproduced from [118] CC BY 4.0.

desaturation, however, the stress change goes to nearly zero, but with some residual deformation preventing it from fully relaxing to the initial state.

4.3. β-to-α phase transition (plateau; delithiation)

The reverse phase transition from β-to-α necessitates the coexistence of both phases during delithiation. Electrochemically, the galvanostatic profile yields a flat delithiation plateau at ~0.45 V vs. Li/Li^+, referring to the β to α phase transformation (figure 7(b)).

Hudak and Huber have suggested that the delithiation processes of Al anodes should be largely responsible for the drastic capacity fading. They observe that the lithiation capacity always matches the delithiation capacity of the previous cycle while the delithiation capacity is usually a fraction of the previous lithiation capacity [61]. Later, an *operando* light microscopy study makes it clear that the delithiation process causes cracks formation within the lithiated regions of **Al thin films**, likely due to the mechanical brittleness of the β-LiAl and volume shrinkage. This electrode damage may induce further embrittlement and loss of material. From SEM images and videos S5–S8, cracks can be clearly observed after delithiation, but are notably restricted within the β-LiAl region (figures 18(a) and (c)). The images for the same regions taken by a BSE detector highlight the distribution of the β-LiAl patch (darker color; figures 18(b) and (d)) [67]. Overall, this process includes elongation of the face-centered cubic Al gains during lithiation (figures 18(e)

Table 2. Lattice parameters and densities of various β-LiAl specimens that are annealed at 500 °C for 168 h. The data are obtained using x-ray diffraction techniques from [78].

Lithium (at%)	Lattice parameter (Å)	Density (g cm^{-3})	Phases
47.8 (±0.3)	6.3593 (±0.0003)	n/a	$\alpha+\beta$
48.3	6.3612 (±0.0004)	1.727 (±0.001)	β
48.9 (±0.5)	6.3639 (±0.0004)	1.725 (±0.002)	β
49.4 (±0.2)	6.3671 (±0.0005)	1.715 (±0.004)	β
49.7 (±0.1)	6.3685 (±0.0003)	1.709 (±0.006)	β
50.3 (±0.1)	6.3710 (±0.0007)	1.708 (±0.001)	β
50.8	6.3743 (±0.0004)	1.702 (±0.001)	β
51.9 (±0.2)[a]	6.3782 (±0.0006)	1.684 (±0.006)	β
52.5 (±0.2)	6.3825 (±0.0007)	1.669 (±0.005)	β
53.9 (±0.7)[a]	6.3870 (±0.0008)	1.647 (±0.008)	β
54.5 (±0.3)	6.3902 (±0.0003)	1.618 (±0.005)	β
56.2 (±0.3)	6.3956 (±0.0012)	n/a	$\beta+\gamma$
∼6.2[b]	∼0.029[b]	∼0.109[b]	β solubility[b]

[a] The specimens are annealed for 96 h instead of 168 h.

[b] The variation of β-LiAl within its solubility range is calculated.

n/a: not applicable due to the coexistence of two phases.

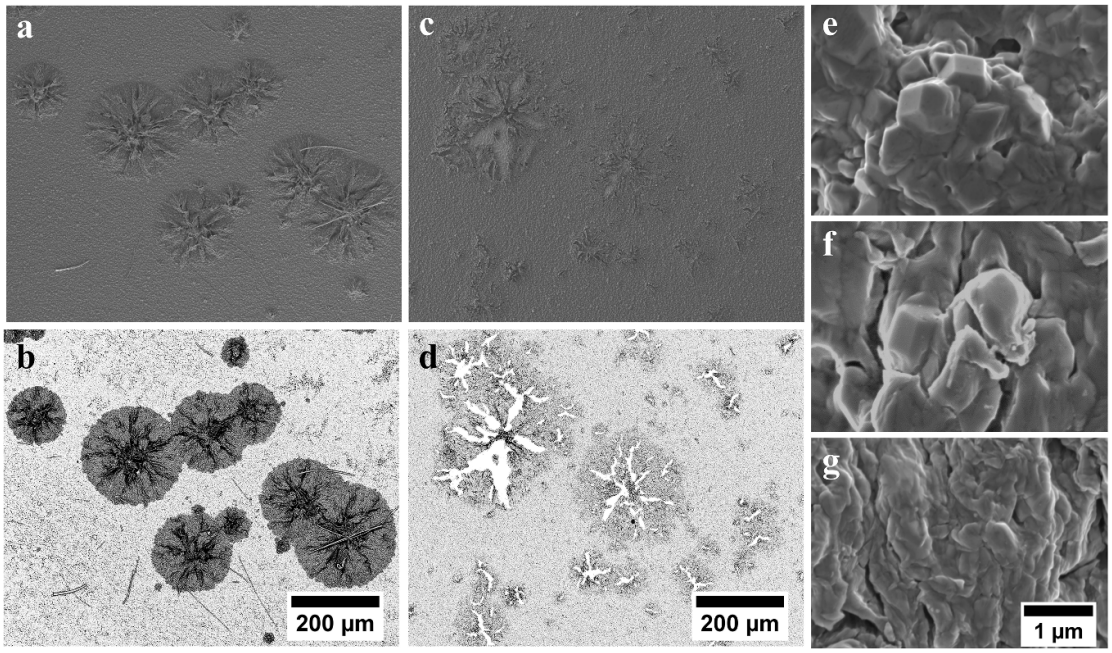

Figure 18. SEM images taken from (a), (b) a partially lithiated and (c), (d) a delithiated Al thin film. (b), (d) Images taken by a back-scattered electron (BSE) detector where the dark circular patches in (b) denote the lithiated β phase LiAl. It appears darker in the image of the BSE detector compared to the surrounding Al due to the lower electron density. High magnification SEM images revealing the grain morphology of I the pristine, (f) the lithiated, and (g) the delithiated Al thin film. Reprinted with permission from [67] John Wiley & Sons. [© 2020 Wiley-VCH GmbH].

and (f)) [80], and a grain rearrangement during delithiation (figure 18(g)), leading to pores left within the delithiated Al matrix.

Although it is suggested that these issues might be less pronounced in **bulk Al foils** without a substrate-electrode interface [67], the formation of pores after delithiation is also observed. While in general, porosity should be expected to be detrimental to the host, as noted in [121], perhaps the process of pore formation can be controlled at the atomic or microscale to avoid degradation. As illustrated in figure 19, if Li is extracted from the lithiated layer in the first delithiation process, the delithiated Al matrix could be self-organized to form a columnar structure with cleavages and micropores.

As discussed before, Al grains become quite small due to the plastic deformation induced by the larger lattice volume of β-LiAl. Therefore, the Al grains should become smaller and smaller after each successive delithiation (figures 11(c) and (d)). This grain refinement process is also evidenced by the *in situ* XRD results. In figure 14(b), it is obvious that the peak intensity of the <111> plane of Al becomes weaker after the first cycle, indicating a weaker crystallinity. By taking a closer look at the full set of diffractograms (figure 14(a)),

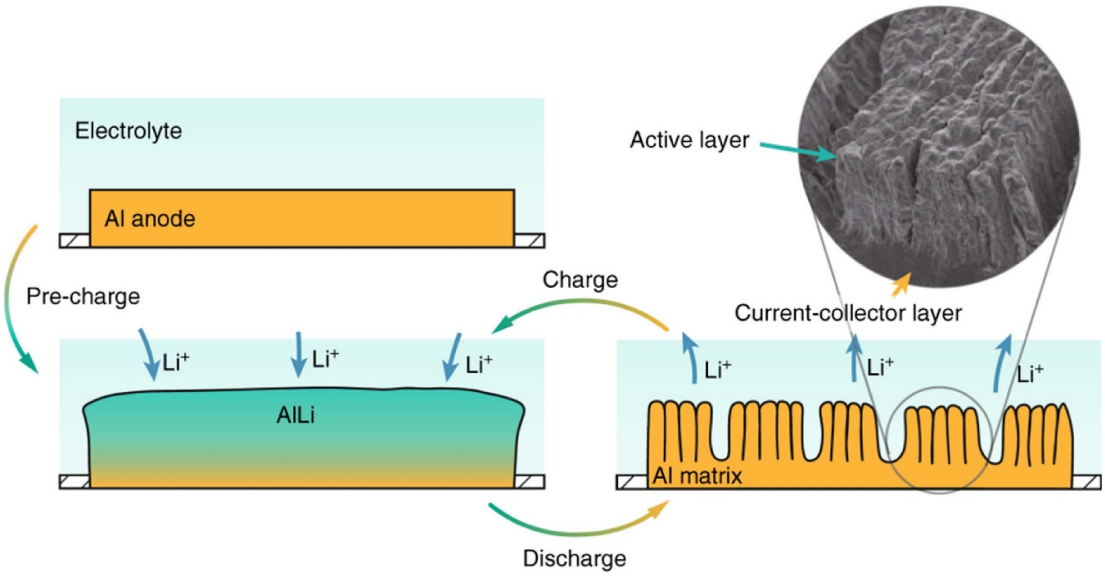

Figure 19. Schematic illustration of how an Al foil anode forms the columnar-porous structure after delithiation. The SEM image is provided to reveal the structure as well. Reproduced from [43] CC BY 4.0.

not only does the intensity of <200> Al exhibit a similar trend, but the peak widths in XRD of both planes seem to be also increased, giving much lower peak-to-width ratios or higher full width at half maximum, which are indicative of smaller crystallite sizes (Scherrer equation). In fact, the delithiated Al is theoretically expected to have a small grain size due to the existence of pores. The typical bicontinuous structure of the porous matrix consists of ligaments or columns, of which the diameter is usually smaller than 1000 nm [121]. Hence, in the case of delithiated Al, the grain size cannot be expected to be larger than this value.

The mechanical stress evolution is surprisingly flat on this delithiation plateau (figure 9(a)), which means that the mechanical stress remains virtually unchanged. Assuming the β-to-α phase transition is ongoing, the stress change should be only limited to the phase interface that is moving through the volume, which should result in a similar mechanical profile as seen with the lithiation plateau. The observed porous Al formation can well explain this constant stress profile during delithiation. The newly formed pores leave a significant number of voids inside the delithiated electrode, which substantially restrict the volume contraction, and thus do not strain the substrate [67]. Just like other dealloying processes, the selective dissolution of an element from an alloy is considered a common approach to producing porous metals [122]. For example, Chen and Sieradzki have provided SEM images of porous Sn, Pb, Cd, and Bi that are fabricated via electrochemical delithiation [121].

5. Subsequent electrochemical cycles ($\alpha \leftrightarrow \beta$)

Although the detailed analyses for the initial cycle help gain fundamental insights into Al anodes, the enablement of Al as an anode candidate for LIBs requires some cyclic stability. For brevity, instead of going through the processes step-by-step, issues and differences stemming from subsequent cycles, in addition to the initial one, are highlighted.

5.1. Secondary SEI formation in liquid cells

The porous structure of the delithiated Al leads to a significant increase in the specific surface area. If liquid electrolytes can penetrate these pores and voids, reaching fresh Al surfaces, then it can be expected that it will facilitate more secondary surface reactions. This secondary SEI formation can partly explain the coulombic inefficiency of Al anodes reported in the literature [59, 61, 106, 123]. It should be noted that these reactions are not one-off processes and would occur as soon as fresh Al is exposed to the electrolyte. When an Al anode is going through repetitive cycles, the surface morphology of the electrode is completely changed (figures 20(a) and (b)), from a flat/dense to a porous/loose structure. At the cross-section (figures 20(c) and (d)), the film thickness expands from several hundreds of nanometers to ca. 20 micrometers (a factor of more than 40), explaining the compressive stress built up over cycling (film thickening) observed in figure 9(b). Taking a closer look at figures 20(e) and (f), the nanostructured Al ligaments and columns will become thinner and thinner due to the irreversible formation of the pores, such that there should be always

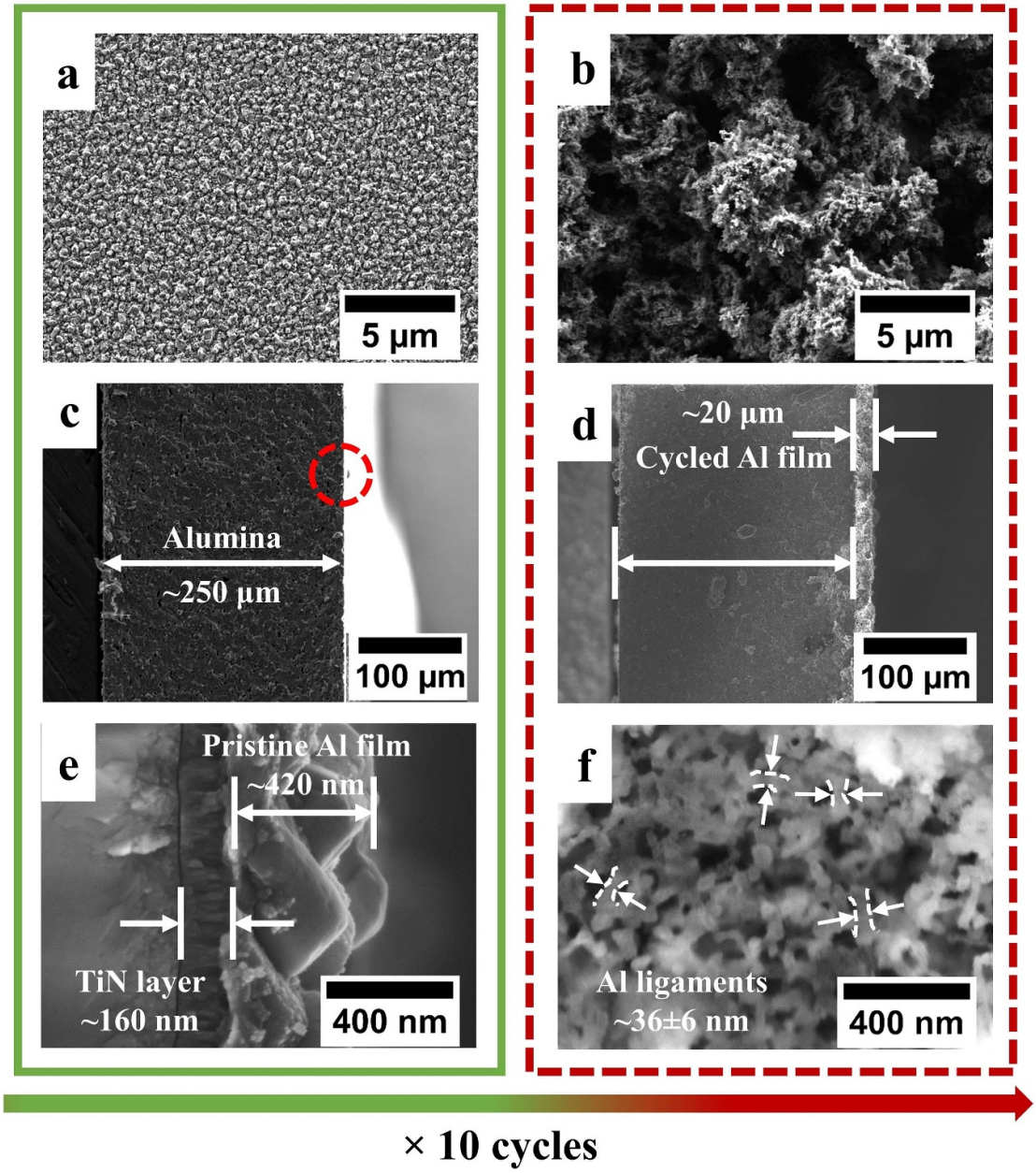

Figure 20. SEM images taken from the Al thin film electrodes before and after cycling: (a), (b) surface morphology taken by a detector for secondary electrons (SE) that is sensitive in probing the height difference; (c), (d) cross-sectional views reveal that the volume expansion of the Al film after 10 cycles is way beyond 100%; I enlarged cross-section of pristine Al film (red dashed circle in (c)) with a thickness of ∼420 nm and (f) enlarged top view of the cycled Al film that exhibits porous features. Reprinted with permission from [67] John Wiley & Sons. [© 2020 Wiley-VCH GmbH].

fresh Al surfaces forming during each delithiation [67]. As a result, an optimized coulombic efficiency is difficult to achieve as long as the formation of porous Al is taking place during each delithiation.

5.2. Ductile-to-brittle transition

Although Al is known to be a soft metal with decent ductility in its original state, a ductile-to-brittle transition is expected in the presence of pores and/or under tension, just like nanoporous gold [124, 125]. This can be evidenced by an interesting SEM image of a partly cycled Al foil. In figure 21, a piece of porous Al (delithiated after ×10 cycles) is falling off from the bulk Al foil, indicating its brittle nature that is more susceptible to deleterious defects. The darker color of the upper (i.e. cycled) layer under a BSE detector indicates a very high level of porosity, where the mean atom density is diluted, thus scattering the electrons less significantly. This observation also allows us to revisit a recent study that relies on backscattered images [35]. The color contrast might not fully indicate the distribution of the β-LiAl but could also be the delithiated Al.

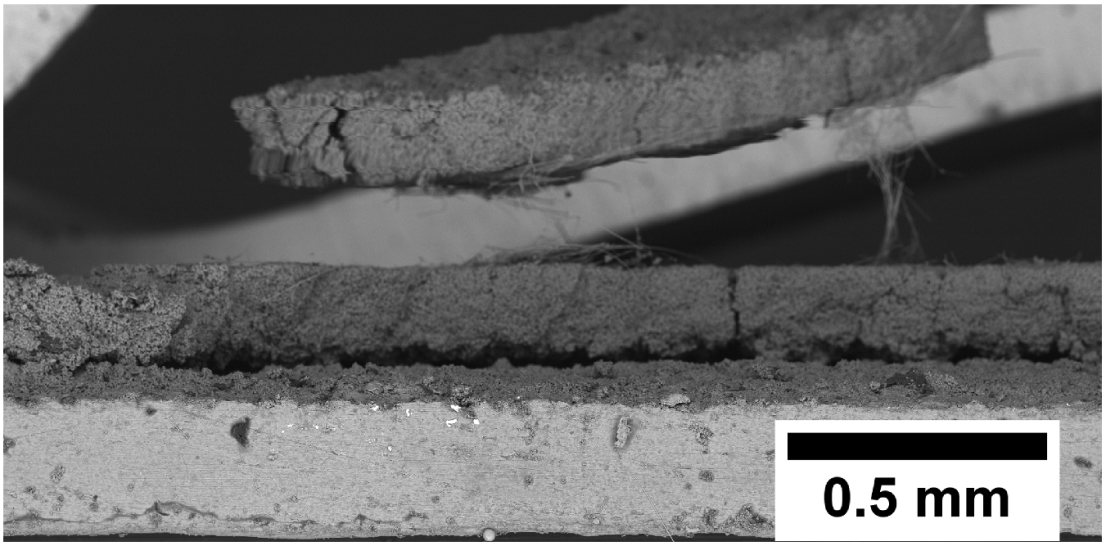

Figure 21. The cross-sectional SEM of a partial cycled (×10) Al foil with an initial thickness of 0.25 mm. The delithiated porous Al expands extraordinarily, becomes brittle, and may fall off from the bulk foil.

Moreover, the brittleness may cause Li trapping issues, which is closely related to the poor cyclability of Al anodes when $\alpha \leftrightarrow \beta$ transitions are engaged. A model developed from the electrochemical data explaining the origin of Li trapping: The delithiation of β-LiAl and the formation of α-Al initiates at the electrode-electrolyte interface while the in-depth β-LiAl may be encapsulated [59]. However, microscopy evidence does not seem to support this model, especially since the β-LiAl is considered a superionic conductor and facilitates fast Li diffusion [84]. Therefore, it is suggested that the loss of active material may be largely responsible for the Li trapping, referring to 'dead Li' rather than the Li encapsulation described in the model.

5.3. Safety concerns

With lithiated Al at room temperature, i.e. β-LiAl, it may be expected to be very reactive to oxygen and moisture due to the high Li content (ca. 50 at%) and perceived to be at risk of safety issues. However, recent studies have highlighted the air compatibility of β-LiAl upon some surface modifications, such as an artificial SEI [126] and a shot-peening treatment [127]. The β-LiAl electrodes with modified surfaces can be quite stable under ambient for several hours. Even when obvious oxidation is observed after days of air exposure, the β-LiAl electrodes are generally stable without any drastic reactions, e.g. smoke or fire. We believe that, reasonably, safety concerns should come from the delithiated Al since there is almost no question that dense Al foils/films in their pristine state would evolve over cycling to form a highly porous Al matrix. Overall, the unsolved problems of Al anodes are all closely related to the formation of pores and seemly intrinsically bonded to the $\alpha \leftrightarrow \beta$ phase transformations. Despite the porosity bringing the problems such as brittleness and volume expansion mentioned above, the huge surface area of the cycled electrode can lead to fire-catching upon air exposure (observed experimentally).

In another safety dimension, the omission of copper current collectors in a full cell with an Al anode raises the prospects for zero-volt stability in a lithium-ion cell. Previously considered a key advantage of Na-ion batteries over lithium, the ability to deeply discharge a cathode, such that the anode potential is raised to that of the cathode will almost certainly lead to the dissolution of copper, evident with $LiFePO_4$ (LFP) cathode cells and made worse with $LiNi_xMn_yCo_{1-x-y}O2$ (NMC) varieties [128]. As presented in figure 22(a), Cu foil is severely corroded when the potential is above ~3.6 V vs. Li/Li^+, as indicated by the sharp CV oxidation peak (~17 mA) and the photographs of the disassembled cell. Not only does the Cu foil pulverize to lose its initial shape, but the corroded Cu powder falls off and sticks to the separator. Whereas Al foil exhibits a much weaker oxidation peak in its cyclic voltammogram (figure 22(b)), even when the α-Al becomes porous, (i.e. delithiated). Furthermore, the appearance of Al foil remains unchanged via eye observation when it is cycled between 1 and 4 V vs. Li/Li^+ (no lithiation of Al) and the CV current is ~1000 times smaller than that of Cu foil (inset of figure 22(b)), indicating its superior stability at the high potentials vs. Li/Li^+ (e.g. an over-discharged full cell).

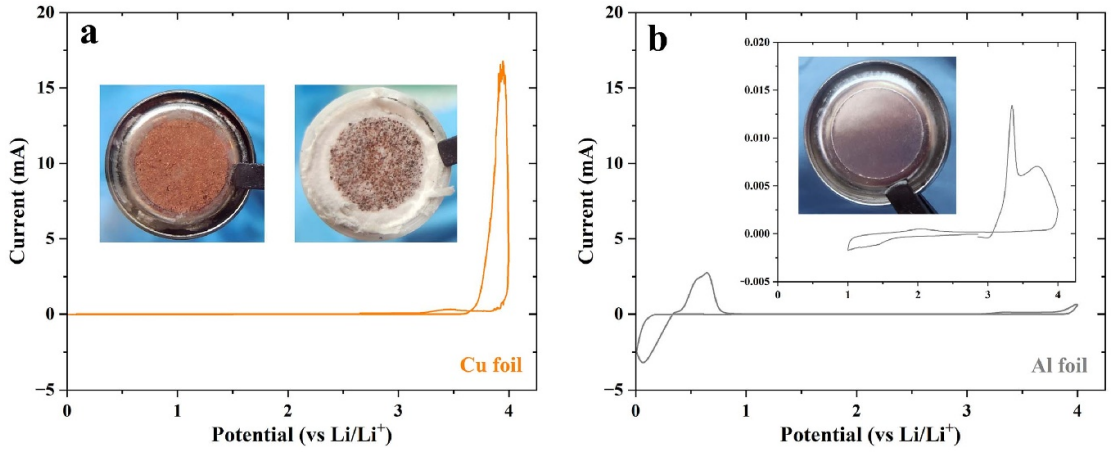

Figure 22. Cyclic voltammograms of (a) the cell consisting of Cu foil vs. Li metal and (b) the cell consisting of Al foil vs. Li metal, with a wide potential range from 0 to 4 V vs. Li/Li^+. The potential range for the inset of (b) is from 1 to 4 V vs. Li/Li^+, to avoid the lithiation of Al at lower potentials.

6. Strategic utilization of Al anodes

By reviewing most of the works that show superior cycling stabilities of Al anodes and comparing them to the ones with poor cycling performances, it can be noted that stable performance of Al anodes is often observed in the full cell configuration [9, 43–47, 129]. When Al anodes are characterized in half cells (i.e. Li metal as the counter electrode), the cycling life is usually restricted to a dozen of cycles [57, 60–62, 67, 80, 95, 106, 107, 123, 130, 131]. With this in mind, it is important to rationalize such behavior in light of the 'full picture' of the Li-Al electrochemical system.

6.1. Origin of anomalous performances

To explain this inconsistency between full and half cells, here we introduce the concept of 'DAU', which is short for 'Degree of Al Utilization'. Ryu *et al* have partly clarified the importance of DAU, and how the DAU affects the cycling performance of Al anodes [46]. Said briefly, the shallower the lithiation depth (or the lesser the DAU), the longer the cycling life of an Al foil is, similar to what has been discussed together with the Maxell $LiMnO_2$-Al cells in figure 2. Several studies have suggested that Al anodes can benefit from partial lithiation because of the heterogeneous nucleation and the ductility of Al [66, 67, 80]. Returning to the inconsistency, the primary difference between a full cell and a half cell is the Li supply. When a Li foil is used as the counter electrode, the Li supply within the half-cell system is considered infinite. As a result, the Al electrodes will be fully lithiated and transformed into the β phase completely, regardless of whether they are films, foils, or composites. Based on the (de-)lithiation mechanisms presented before, it seems quite reasonable that the Al anodes fail prematurely in these half cells. Yet in a full cell, the Li amount is limited by the cathode. If one carefully revisits the above-mentioned full cell studies that give several hundred stable cycles, the DAUs are usually very low, e.g. 5.5% and 3.5% [44]. This means that most of the Al anode is still fresh Al, which is mechanically more stable and capable of storing significantly more Li, and additionally acts as a consumable Al source, allowing for a minor, but effectively undetectable degradation with each cycle. It is therefore not surprising that a stable cycling performance is achieved. All these DAUs are extracted and summarized in table 3 together with the cell parameters to allow easy comparisons. It then seems logical that a lesser DAU should give a better cycling life to Al anodes, or to any other electrode materials, which helps explain why long cycling is only observed from the full cells with Al anodes, but not from the half cells.

Considering the situation, Chen *et al* try to benchmark the degradation behavior of Al foil anodes for LIBs, by testing a total of 60 half cells. In figure 23(a), a correlation is established between the number of cycles before failure and the areal capacity per cycle of Al anodes, which, in general, agrees with a better cycling life at a lesser DAU or vice versa. More specifically, figure 23(b) presents the same data, but with both axes in the logarithmic scale. Regardless of whether Al foils are pure or alloys, the correlation seems linear with error bars obtained from multiple cells. Upon understanding why and how DAU affects the performance of Al anodes, the vital role of prelithiation can also be highlighted in full cell applications. If an Al anode is not prelithiated, a certain amount of Li atoms from the cathode may be trapped (e.g. cyclic SEI) during the delithiation of β-LiAl, and subsequently resulting in cell degradation. Pre-storing Li atoms into

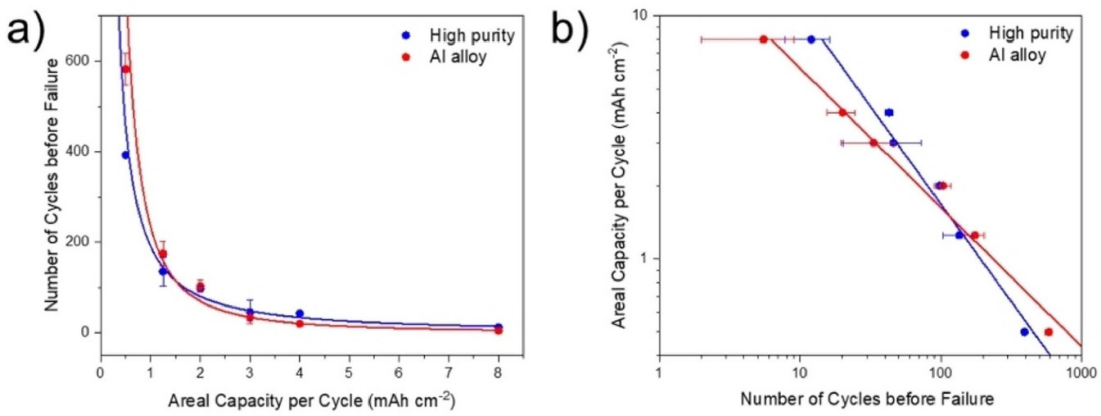

Figure 23. Compiled electrochemical cycling behavior and electrochemical fatigue mechanism. (a) Number of cycles before failure vs. the areal capacity per cycle for both types of foil; the number of cycles to failure exhibits a strong dependence on areal capacity. Each data point is the average of multiple cells running to failure, with the error bars showing standard deviation. (b) Logarithmic plot of the data in (a) with the axes exchanged to show similarity to lifetime plots in mechanical fatigue analysis. Lines are linear fits. Reprinted with permission from [34] John Wiley & Sons. [© 2022 Wiley-VCH GmbH].

Table 3. Parameters of the full cells that show promising cycling lives of Al foil anodes. The term DAU refers to the 'degree of aluminum utilization'.

Full cell components	Cathode capacity (mAh cm^{-2})	Anode capacity (mAh cm^{-2})	Calculated DAU (%)	Cycle life	References
$LiCoO_2$-Al	~2	~18 (67 μm)	11	120; No degradation	[43]
$LiCoO_2$-Al	~0.44	~5.4 (20 μm)	5.5[a]	250; 81% retention	[44]
$LiNi_xMn_yCo_{1-x-y}O2$-Al	~0.47	~5.4 (20 μm)	5.9[a]	250; 86% retention	[44]
$LiFePO_4$-Al	~0.27	~5.4 (20 μm)	3.5[a]	500; 84.2% retention	[44]
$LiFePO_4$-Al	~0.99	~13.4 (50 μm)	6.6[a]	200; 88% retention	[45]
$LiFePO_4$-Al	~1.4	~5.4 (20 μm)	26	200; No degradation	[46]
$LiFePO_4$-Al	~2.84	~5.4 (20 μm)	53	35; 88.7% retention	[46]

[a] The sizes of the anode and the cathode are different.

the Al anode (i.e. prelithiation) can effectively mitigate this issue since Li stock should no longer be a limiting factor. More details regarding prelithiation techniques can be found in § 6.3.

Overall, a low DAU might not be acceptable for some anode candidates since it directly dilutes the specific capacity of a full cell. Al foil anodes, however, should be critically assessed due to the unique situation that they can potentially function as both active material and current collector. More importantly, the usage of Cu element can be completely omitted in the cell, leading to a roughly one-fifth reduction in material cost [132], while electrode manufacturing is expected to be simplified [10]. Cu is known to be a relatively dense metal with a density of 8.96 g cm^{-3}, which is about 3.3 times higher than that of Al. These facts may make the Al foil anodes with relatively low DAUs acceptable in real applications, especially since the elimination of electrochemically inactive components (e.g. Cu foil, binder, etc) provides extra room for allocating more Al in the LIB cell design.

6.2. Mechanical strain engineering

On the other hand, some studies in table 3 show great promises in real applications, regardless of the DAUs. Hong Li has done a practical evaluation of LIBs and stated clearly that the areal capacity of commercial batteries is 3–4 mAh cm^{-2}, likely by considering two sides of the electrode [12]. Therefore, the $LiCoO_2$-Al cell made by Li *et al* [43] can be quite competitive by delivering ~2 mAh cm^{-2} one-side capacities without capacity fading after 120 cycles. By taking a closer look, their work draws some explanatory illustrations that help the readers easily understand the lithiation mechanisms of different Al foils (figure 24). Two modes are proposed here: (1) when uniform lithiation is achieved, the mechanical strain generated by volume expansion is mostly elastic and restricted at the phase interface, such that the overall electrode integrity is properly maintained (left column); (2) when a stochastic lithiation occurs at the surface, huge strains are generated locally causing dislocations, and eventually pulverization of the electrode (right column). The core finding here is that the Al foil electrode with the uniform lithiation pathway may circumvent catastrophic, localized strains. Although this was illustrated with strain engineering, selective doping or alloying, may offer

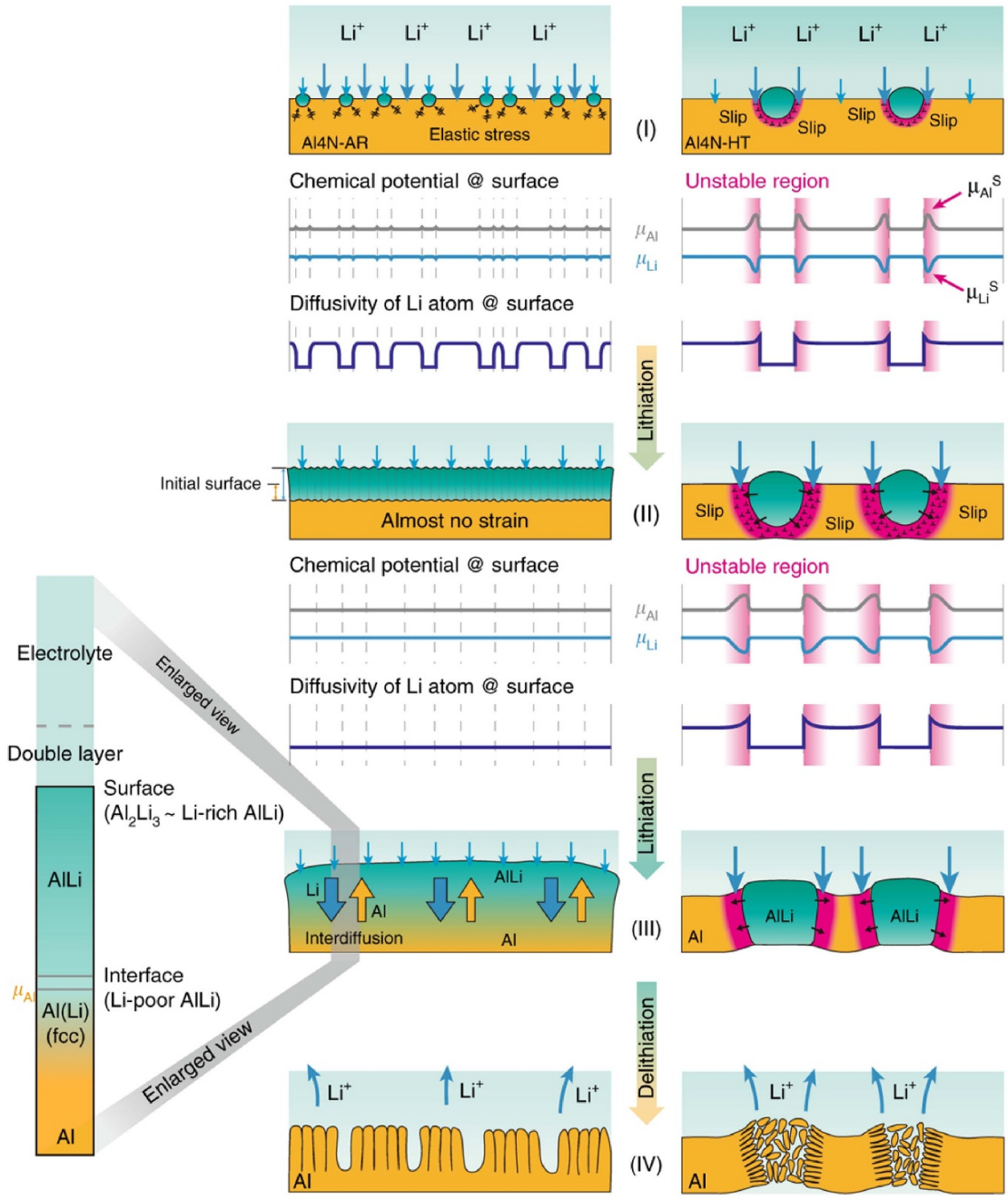

Figure 24. Schematic illustration of the lithiation processes of mechanically hard (as rolled; 99.99% purity) and soft (annealed; 99.99% purity) Al foils. The appropriate hardness of the as rolled Al foil enables homogeneous lithiation. Reproduced from [43].

a chemical pathway. For instance, additions of Mn or Cr are known to improve the cycle life of Al anodes [56], but further studies are certainly warranted. Nevertheless, it is clear that, under the right circumstances, the $\alpha \leftrightarrow \beta$ phase transformations can be quite stable during cycling.

Extending some of these concepts to lithium-ion solid-state batteries, the underlying phase transformations should be equivalent to liquid cells. However, the intense applied compressive stress combined with solid electrolytes could change the strategy for the utilization of Al as an anode material. Particularly considering a recent work by Sakka *et al* the significant void volume fraction in powder-based solid-state cells is inversely related to externally applied pressure, as shown in figure 25(a) [133]. Taking a closer look, this stack pressure will translate to the pressures among circular particles that are several orders of magnitude higher due to extremely low contact areas (figure 25(b)).

Following this, it has already been noted with *in situ* x-ray tomography with CuS (also prone to expansion during lithiation) that 'crack formation could be effectively suppressed by increasing the stack

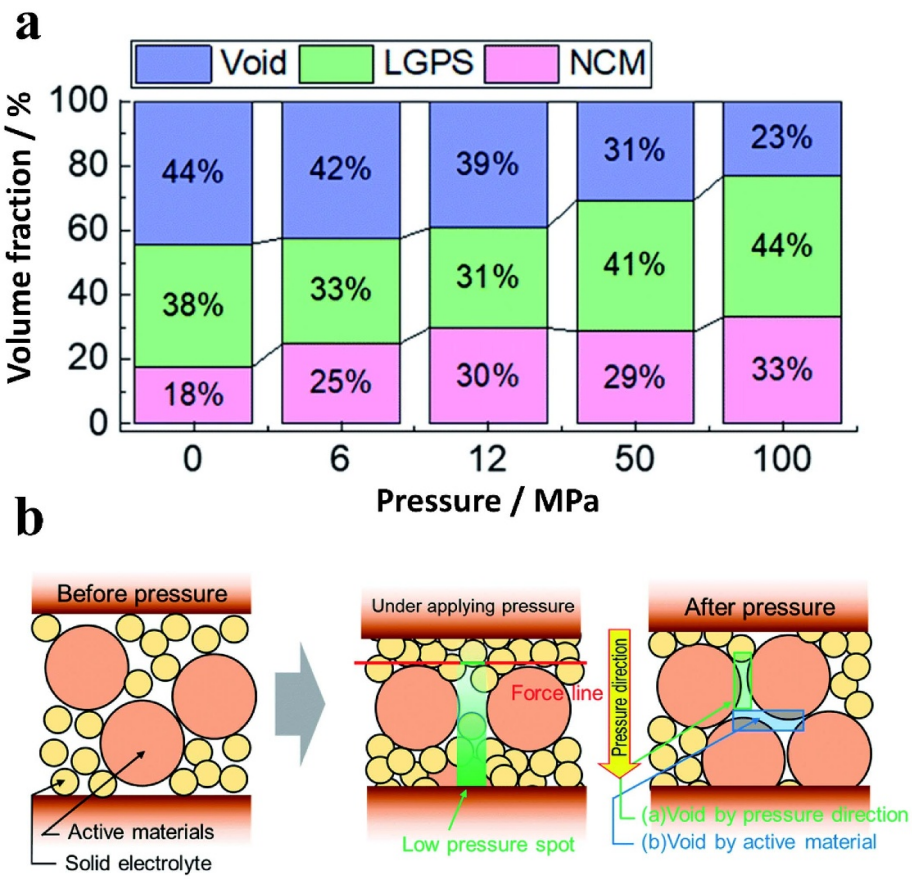

Figure 25. (a) Volume fraction of $LiNi_{0.33}Co_{0.33}Mn_{0.33}O_2$ (NCM), $Li_{10}GeP_2S_{12}$ (LGPS), and voids in the composite electrode layer for various pressures. (b) Schematic illustration of morphological structural changes in a composite electrode by pressure application. Reproduced from [133]. CC BY 3.0.

pressure from 26 to 40 MPa' [134]. Further complicating the strain scenario is the contribution from internal expansion. For micro Si, this could reach ∼62 MPa and for LiIn, this was measured and estimated to be ∼6 MPa of axial stress (after accounting the for the mismatch between the calculated and experimental values (figure 26(d)) [135], similar to what was measured for CuS [134]. This strongly supports the concern that the delicate mechanical aspects of moving through the relevant phases of the Li-Al system with its range of structures and properties. Adding to this is the interesting case of β-LiAl, which is known to increase its hardness (figure 13(a)) [115] and yielding strength (figure 13(b)) [64] as lithium content is increased within its solubility range. Therefore, the prospects for Al anode utilization in a solid-state battery certainly warrant further research and exploration.

6.3. Prelithiation

Prelithiation is known as one of the common ways to improve the performance of Li-based energy storage systems [126, 129]. Ryu *et al* presented a facile but effective method to prepare the prelithiated LiAl anodes for LIB applications. As illustrated in figure 27(a), Li and Al foils are mechanically pressed together to form the LiAl alloy using a liquid electrolyte as the intermediate. The LiAl grains are characterized to be nanocrystalline (figures 27(b) and (c)). At the cross-section (figures 27(d)–(f)), a very homogeneous layer of the β-LiAl can be observed on top of the Al foil. Such a mechanically prelithiated Al anode delivers 200 stable cycles when pairing with an LFP cathode. It should be mentioned that the DAU of the Al anode is ∼26%, which is the highest among all the Al anodes with cycle lives longer than 100 [46]. Not only does the mechanically prelithiated Al anode give impressive cycling performance at a relatively high DAU level, but more importantly, the facile preparation method can easily be scaled up to fulfill industrial requirements. In the absence of mixing-pasting-baking processes, the fabrication of this Al-based anode becomes more competitive both financially and technically. Additionally, labor costs and energy consumption can be potentially reduced without sophisticated heating processes [10].

Of course, prelithiation is not without trade-offs, particularly when most of the lithium is used in the anode for what is effective for structural purposes (stabilization of β-LiAl, described below in § 6.4). For

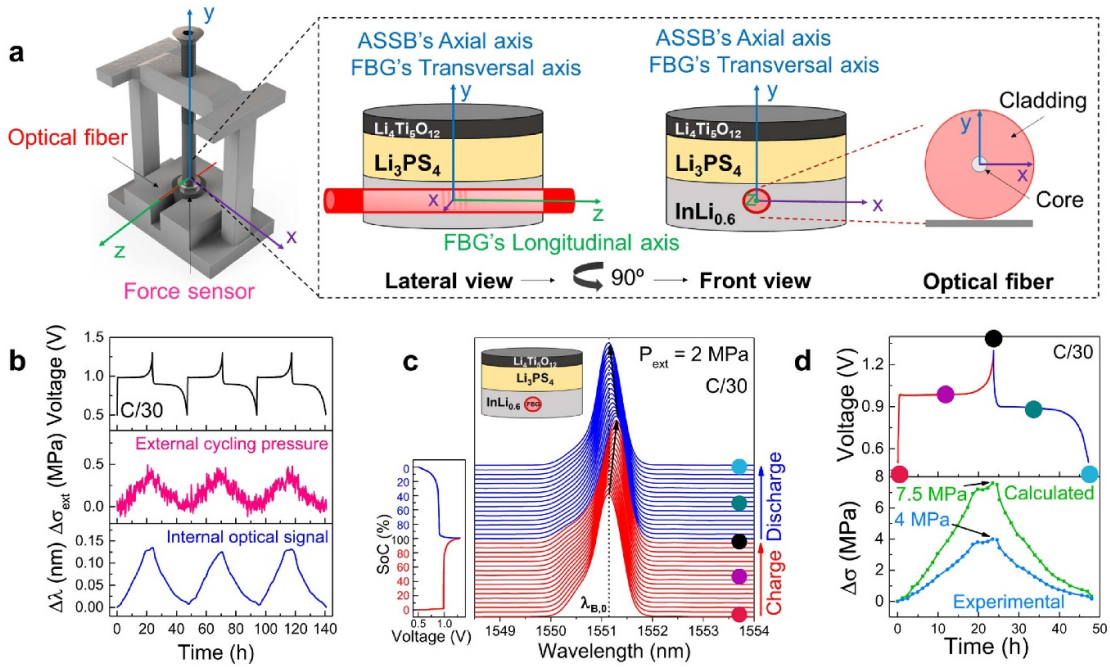

Figure 26. *Operando* Li-driven stress monitoring in InLix | LPS | LTO cell by an FBG embedded in the anode. (a) Scheme of the modified coin cell with the implemented optical fiber and the external force sensor. The corresponding *X*-, *Y*-, and *Z*-axis are detailed in the different views. It is important to note that an axis transverse to the fiber is an axis perpendicular to the main symmetry axis (c∞) and therefore the axis 'axial' to the cell is a 'transverse' axis to the fiber. To simplify nomenclature, every time we herein mention 'longitudinal' or 'transversal' will be respected to the fiber and 'axial' will only be respected to the cell. (b) Time-resolved voltage (top), external cycling pressure (middle), and an internal optical signal (bottom) for the aforementioned ASSB cycled at C/30 (5.83 mA g^{-1}) and 25 °C in an operando mode. (c) 2D stack view of the reflected spectra, with the corresponding galvanostatic charge/discharge cycle. The charge and discharge processes are plotted in red and blue, respectively. (d) Comparison between operando stress evolution obtained: 1—internally by the FBG sensor and using the mathematical model (green curve) and 2—internally by the FBG sensor and the sensitivity coefficient obtained with the experimental calibration of the sensor (blue curve). The respective galvanostatic charge/discharge is presented (top). The points at the beginning/middle/ end of the charge/discharge are indicated by colored dots, also marked in the corresponding FBG spectra in (d). The external cycling pressure was fixed at 2 MPa prior to performing the battery cycling. Reproduced from [135]. CC BY 4.0.

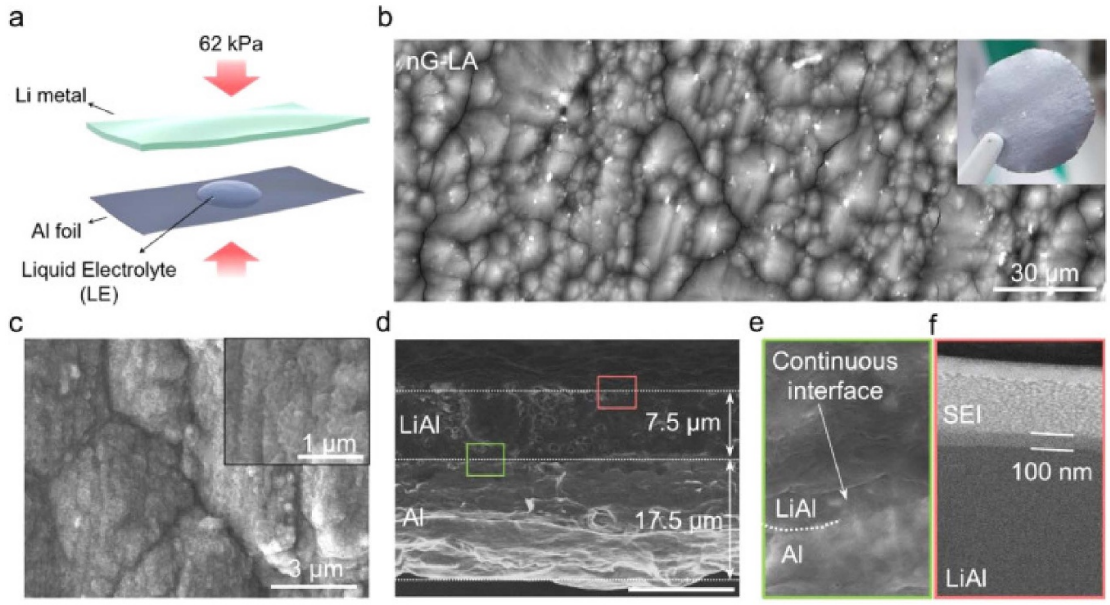

Figure 27. Design of electrolyte-mediated mechanical prelithiation (EMP) method and resulting LiAl layer with a Li concentration gradient and nanograins (nG-LA). (a) Schematic of nG-LA preparation. (b), (c) Top-view SEM images of nG-LA at different magnifications (inset: Enlarged SEM image of selected area). (d)–(f) Cross-sectional SEM image of nG-LA (Scale bar: 10 μm for (d)), showing a continuous interface between the LiAl layer and bare Al (e), and SEI layer thickness of 100 nm on the LiAl layer by dual-beam FIB combined with SEM (f). Reprinted from [46], Copyright (2020), with permission from Elsevier.

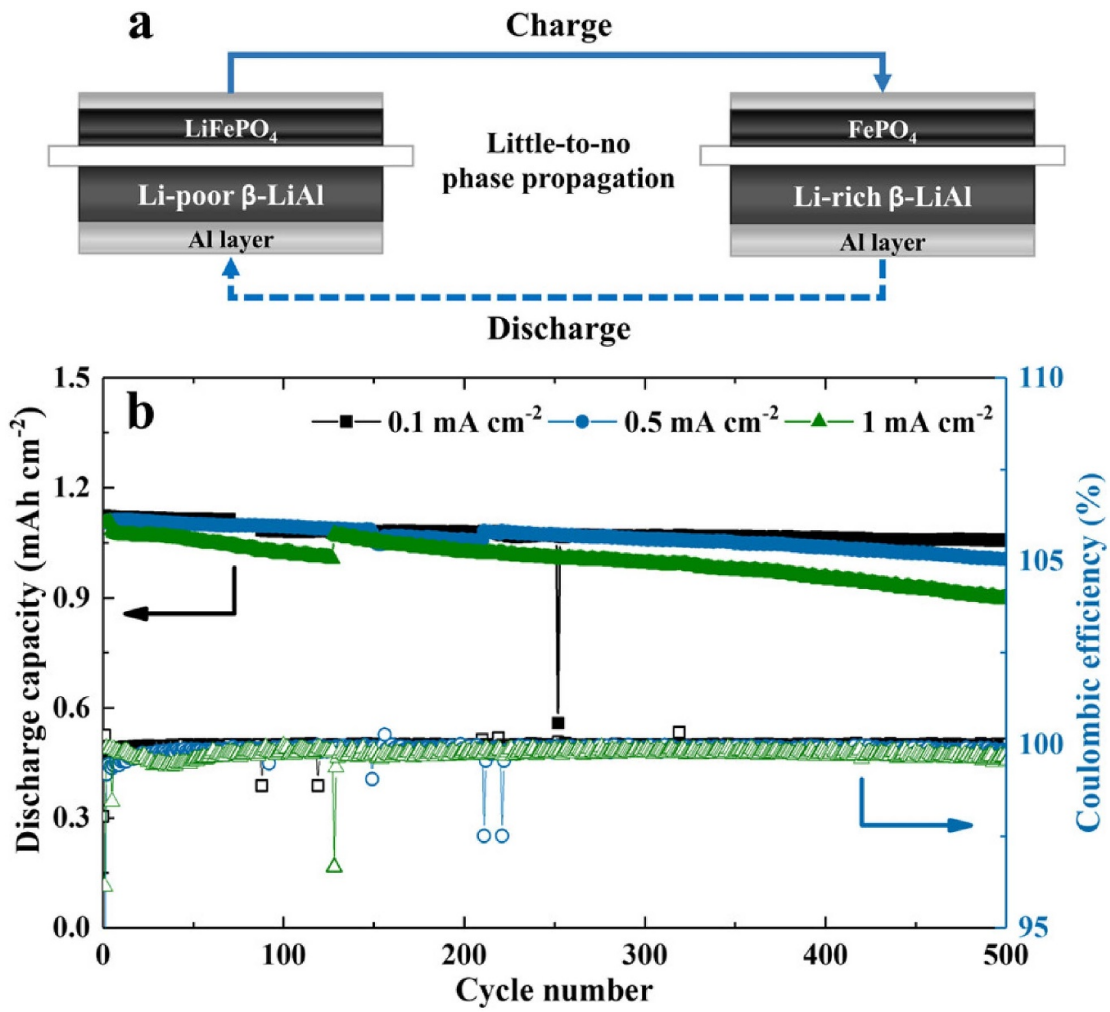

Figure 28. (a) Schematic illustrations of a novel full cell design using the β-LiAl grown on an Al foil as an anode and a commercial LFP cathode. (b) Cycling performance obtained at various current densities when the cathode capacity is below the one contributed by the solubility range of the β-LiAl anode. Reproduced from [9]. CC BY 4.0.

example, an anode that is limited to β-LiAl can have ~6% at use for reversible cycling capacity, but ca. 48 at% Li must be used just to form the Zintl structure first. This factor of ×8 for inactive Li is certainly a detractor from the other advantages of this electrode material.

6.4. Utilization of β-LiAl solubility

A scientific aspect regarding the Li solubility range of the β-LiAl should be considered, especially for prelithiated Al anodes. As already discussed, the β-LiAl layer of a prelithiated Al foil should exhibit a solubility range that can potentially give a capacity of ~242 mAh g^{-1}-Al without a phase transformation. When the β-LiAl crystal structure is maintained (illustrated in figure 28(a)), the cycling life should be theoretically infinite since the issues caused by the $\alpha \leftrightarrow \beta$ phase transformations, such as localized strain, pores formation, and secondary SEI formation, are circumvented or mitigated (~1.4% volume expansion can be expected between the ends of the β-LiAl solubility range). Figure 28(b) shows the experimental evidence for the argument above, where 500 stable cycles are achieved at various rates for a partly lithiated Al foil. Through reviewing the details from the study, the DAU of the system is translated to be only ~2%, but it offers a unified understanding of why Al anodes sometimes last hundreds of cycles in full cells. Also, the study suggests that the DAU can be further increased (an optimum value should exist) but necessitates systematic investigations. For instance, a control experiment was done in the same study using a 0.18 mm Al foil to replace the original 0.25 mm one without changing the prelithiation depth (i.e. 0.1 mm is prelithiated) and other cell components, yet both exhibit similar cycling performance [9].

Apart from the applications in various devices, the role of solubility range can also help shed light on the cycling performances summarized in table 3. For the full cell with a DAU lesser than 20%, the solubility range of the β-LiAl should be the primary capacity source, thus giving the Al anode a long cycling life. This

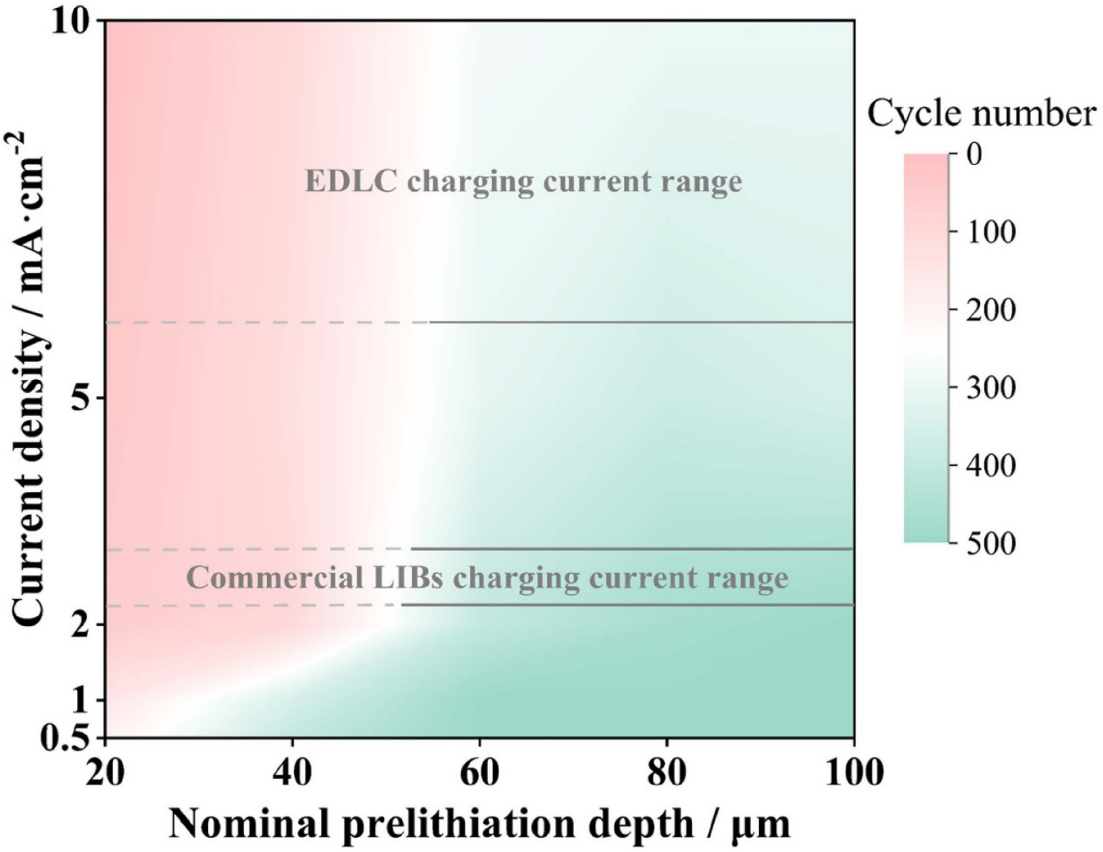

Figure 29. Mapping of cycle life for $Li_4Ti_5O_{12}$//β-LiAl(Al) cells prior to ⩾80% capacity retention at different current densities. The horizontal lines indicate the common charging current densities for commercial EDLCs and LIBs, considering cell areal capacity of ∼1.5–2 mAh cm^{-2} (single-side) and the common charging C-rate of 1.5 C. [85]. Reprinted from [85], Copyright (2023), with permission from Elsevier. CC BY 4.0.

hypothesis may be partly supported by the evident difference between the theoretical and the reversible capacity in one of the studies [44]. For instance, the $LiCoO_2$-Al, NMC-Al, and LFP-Al should have theoretical capacities of ∼270 mAh g^{-1}, ∼284 mAh g^{-1}, and ∼170 mAh g^{-1}, respectively, normalized to cathode mass. However, the reversible capacities for the three cells are ∼160 mAh g^{-1}, 170 mAh g^{-1}, and 126 mAh g^{-1} [44], suggesting that not all the lithium in the cell is being utilized and the β-LiAl solubility likely plays important roles in these cells.

Regarding the volumetric capacity of β-LiAl, the headline figures are likely not as attractive as it is an insertion/intercalation material. By its nature, this phase is acting as a scaffold for the reversible insertion of Li and thus with only ca. 6 at% of the crystal used for cycling, the number of charges stored per unit volume of the host will not compete with conventional anodes, e.g. graphite. However, the limited volumetric capacity comes with minimal volumetric expansion and relatively fast Li transport. Hence the value proposition of a β-LiAl anode is unlikely to compete directly with alloy anodes in the same application space and/or cell design. Perhaps a better comparison in this regard is with respect to lithium titanate ($Li_4Ti_5O_{12}$), which is also an insertion material with minimal volume expansion and despite no longer being used in EVs, is still seeing healthy market growth by Toshiba for ferry electrification and stationary power supplies.

6.5. Targeting effective-immortality of β-LiAl

Regardless of whether the Li solubility range of β-LiAl plays a primary role, a 'user guide' for prelithiated Al anodes is provided in figure 29. This demonstration is built upon a full cell design using $Li_4Ti_5O_{12}$ (high rate capability, high cycle stability) and β-LiAl(Al) as the cathode and the anode, respectively. The cell capacity is roughly 1.25 mAh cm^{-2}, determined by the theoretical capacity of the commercial $Li_4Ti_5O_{12}$ electrode (NEI Corporation). Through cycling 25 cells with various charging currents and anode prelithiation depths, it is suggested that, considering ⩾80% capacity retention after 400 cycles as a key indicator, Al anodes with a nominal prelithiation depth lower than ∼50 μm (i.e. 50 μm Al is lithiated) only survive under low-rate charging conditions (below ∼2 mA cm^{-2}). When the prelithiation depth is increased to higher than ∼50 μm, however, the charging rates seem less relevant, giving ⩾300 cycles at a rate as high as 10 mA cm^{-2}.

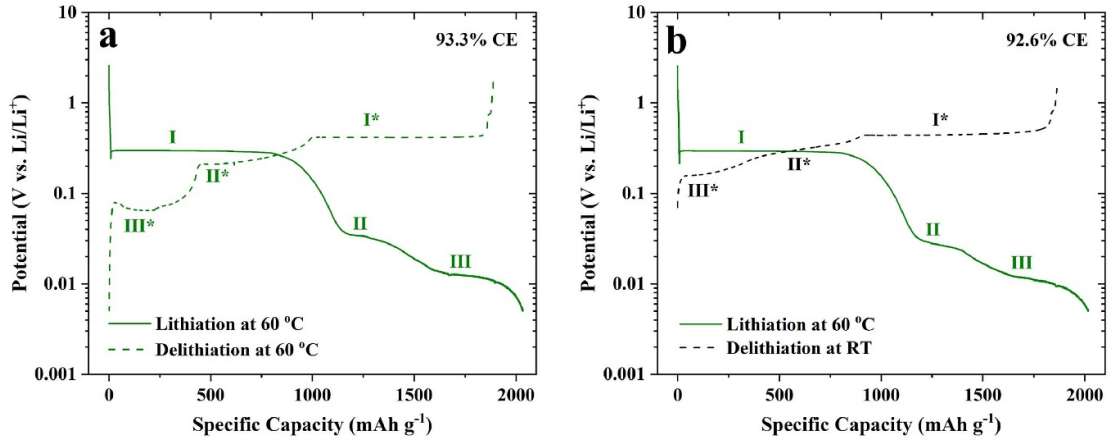

Figure 30. Galvanostatic profiles of the Al thin film electrodes that are lithiated at 60 °C and delithiated at (a) 60 °C and (b) at room temperature (RT). Reproduced from [118]. CC BY 4.0.

The variations in performance are suggested to directly stem from Li diffusivity in β-LiAl. Overall, figure 29 highlights different ways of using Al anodes aiming at different application purposes. For instance, a low prelithiation depth may be sufficient for batteries that are always charged at low rates. Yet, when targeting the effective-immortality of an Al anode, higher prelithiation depths and low charging rates are suggested to be always beneficial, as the β-LiAl solubility is the main contributor for Li (de-)intercalation (i.e. no phase transformations). The raw cycling data can be found in the original work [85].

6.6. Asymmetric thermal behavior

Whether the investigation on Al anodes in LIBs should remain focused on the β-LiAl phase or shift to the Li-rich phases with much higher capacities will depend on the application requirements. A thermally asymmetric feature, nevertheless, should indeed be clearly stated: *only the lithiation process necessitates slightly elevated temperatures to form Li-rich phases*. As shown, once the $Li_{2-x}Al$ phase is formed by lithiating an Al film anode at 60 °C, it can be delithiated to form the α phase and deliver similar levels of delithiation capacity at both 60 °C (figure 30(a)) and room temperature (figure 30(b)).

Importantly, this asymmetric thermal behavior may be ideal for some applications, considering that the lithiation of the anode is equivalent to the charging process of a full cell. For EVs, the heat accumulation during charging is not necessarily a negative thing, as it can warm up the battery pack in winter and facilitate a faster ion diffusion that positively affects the charging speed and reduces lithium plating risks. With an Al anode, the low-grade waste heat generated during the charge due to internal resistance may already be sufficient to facilitate the formation of Li_3Al_2 and $Li_{2-x}Al$ phases. Another example could be the solar farm, which captures energy from sunlight. Solar energy can be more effectively utilized if the excess energy during the daytime or sunny days gets stored in energy storage devices like LIBs and is reused whenever necessary, e.g. during nights or cloudy days. The temperature is often higher when the sun is shining intensively during the daytime, which may create more ideal conditions for Al anodes to form Li_3Al_2, $Li_{2-x}Al$ phases, or even Li_9Al_4 during the charging process. In both cases, although discharge mostly occurs at relatively low temperatures, it is not an issue due to the electrochemical asymmetry presented here.

7. Conclusion, perspectives, and prospects

To summarize, despite the long history of Al anodes in LIBs, there is still much to learn about the prospects of Li_xAl electrodes as the scale of energy storage devices pushes to unprecedented levels. Scientifically, a conclusive plot (figure 31) is shown at the end of this report, to offer a full picture of how Al behaves as an anode material in LIB systems. For lithiation, in addition to the well-studied α-to-β phase transformation (first plateau), the role of the β-LiAl solubility range has been elaborated to give a specific capacity of 1152 mAh g^{-1} upon the formation of Li-rich β-LiAl. More importantly, Li_3Al_2 and $Li_{2-x}Al$ are reported to be formed at temperatures slightly above ambient, doubling the well-adapted specific capacity of $\sim$993 mAh g^{-1}. The formation of Li_9Al_4, on the other hand, seems to be governed by a different mechanism and exhibits a higher nucleation barrier, partly explaining why it is not approachable at the temperatures that facilitate the formation of Li_3Al_2/$Li_{2-x}Al$. Moving to delithiation, Li_9Al_4-to-$Li_{2-x}Al$ and $Li_{2-x}Al$-to-Li_3Al_2 phase transformations seem to occur simultaneously, yielding one plateau until the nucleation of Li_3Al_2.

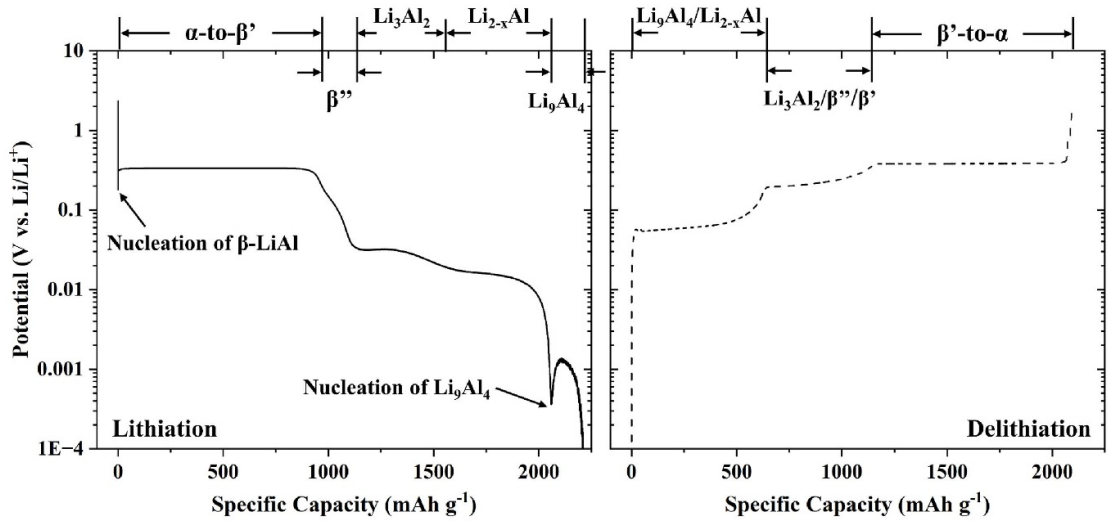

Figure 31. A galvanostatic profile obtained from a 30 μm thick Al foil at 50 °C and an extremely slow rate (C/100 considering β-LiAl capacity; ~450 h for a complete cycle), presenting a full picture of the Al anode with features annotated. β' and β'' denote the Li-poor and the Li-rich β-LiAl, respectively. The annotations on top of the plot refer to the phases being formed (lithiation) and the phases being transformed (delithiation).

Similarly, the delithiation of Li_3Al_2 and desaturation of β'' are also ongoing at the same time. Together with the asymmetric thermal behavior reported in this review, lithiation/delithiation kinetics of the higher-order phases are suggested to be of primary interest and warrant further investigations. Regarding the reversibility of these Li-Al phases, cycling between β-LiAl and $Li_{2-x}Al$ is significantly more stable than cycling the commonly adapted $\alpha \leftrightarrow \beta$, which induces the formation of porous Al and must be controlled.

From a macroeconomic perspective, the levels of production forecasted for the coming years would imply looming differentiation in the sector, circumventing the need for a one-size fits all vision for future LIBs. That being said, the first mover advantage of Si as *the* future anode material should not be understated. With billions of dollars and reputations banked on a future of LIBs containing composite, slurry-coated electrodes, the introduction of a disruptive foil-based platform faces a significant activation energy. Alas, at this stage many investment decisions are no longer made by those who are technology-driven, but rather by those with alternative ambitions. Nevertheless, methods like prelithiation are certainly an emerging necessity in the world of Si-rich anodes, but as is also needed for forming and maintaining the β-LiAl phase in Al foils, thus synergy between these elemental platforms certainly exists. In the end, it may be up to yet-another battery startup company to champion Al before the gigafactories of the world reorient themselves.

Further still, as the value cycle of LIBs comes under closer scrutiny in the West, the prospects for cells with low criticality should be expected. However, this cannot be expected to happen in a vacuum, and thus the rising prominence of post-Li technologies, such as Al-ion or Na-ion, is growing immensely in the battery community due to its prospects for good performance and better sustainability (vis-a-vis material and production costs, in theory). We must then ask the question, how can Al be utilized more in LIBs to such that an Al-rich foil anode be coupled with a cathode that is equally simplified, and in what format should this be packaged? Such are the open questions that remain, but certainly, the answers will only be found by thinking outside of the *baux*.

Data availability statement

All data that support the findings of this study are included within the article (and any supplementary files).

Acknowledgments

Tianye Zheng gratefully acknowledges the 'PolyU Distinguished Postdoctoral Fellowship Scheme' (1-YWBT) and the support from Professor Wei Jin at The Hong Kong Polytechnic University (PolyU). Steven T Boles acknowledges the ENERSENSE research initiative (68024013) at Norwegian University of Science and Technology (NTNU), Norway. The authors are thankful to Dr Dominik Kramer and Dr Reiner Mönig from

the IAM-MMI of Karlsruhe Institute of Technology (KIT), Germany, for numerous helpful technical discussions.

ORCID iDs

Tianye Zheng https://orcid.org/0000-0002-2281-9506
Steven T Boles https://orcid.org/0000-0003-1422-5529

References

[1] Yoo H D, Markevich E, Salitra G, Sharon G and Aurbach D 2014 On the challenge of developing advanced technologies for electrochemical energy storage and conversion *Mater. Today* **17** 110–21
[2] Lee Y J, Yi H, Kim W J, Kang K, Yun D S, Strano M S, Ceder G and Belcher A M 2009 Fabricating genetically engineered high-power lithium-ion batteries using multiple virus genes *Science* **324** 1051–5
[3] Johansson P, Alvi S, Ghorbanzade P, Karlsmo M, Loaiza L, Thangavel V, Westman K and Årén F 2021 Ten ways to fool the masses when presenting battery research** *Batter. Supercaps* **4** 1785–8
[4] Frith J T, Lacey M J and Ulissi U 2023 A non-academic perspective on the future of lithium-based batteries *Nat. Commun.* **14** 420
[5] Boles S T and Tahmasebi M H 2020 Are foils the future of anodes? *Joule* **4** 1342–6
[6] Obrovac M N and Chevrier V L 2014 Alloy negative electrodes for Li-ion batteries *Chem. Rev.* **114** 11444–502
[7] Obrovac M N 2018 Si-alloy negative electrodes for Li-ion batteries *Curr. Opin. Electrochem.* **9** 8–17
[8] Obrovac M N, Christensen L, Le D B and Dahn J R 2007 Alloy design for lithium-ion battery anodes *J. Electrochem. Soc.* **154** A849
[9] Zheng T, Kramer D, Mönig R and Boles S T 2022 Aluminum foil anodes for Li-ion rechargeable batteries: the role of Li solubility within β-LiAl *ACS Sustain. Chem. Eng.* **10** 3203–10
[10] Zheng T and Boles S T 2022 Simplifying electrode design for lithium-ion rechargeable cells *ACS Omega* **7** 37867–72
[11] Gogotsi Y and Simon P 2011 True performance metrics in electrochemical energy storage *Science* **334** 917
[12] Li H 2019 Practical evaluation of Li-ion batteries *Joule* **3** 911–4
[13] Cheng X B, Zhang R, Zhao C Z and Zhang Q 2017 Toward safe lithium metal anode in rechargeable batteries: a review *Chem. Rev.* **117** 10403–73
[14] Su X, Wu Q, Li J, Xiao X, Lott A, Lu W, Sheldon B W and Wu J 2014 Silicon-based nanomaterials for lithium-ion batteries: a review *Adv. Energy Mater.* **4** 1300882
[15] Ko M, Chae S and Cho J 2015 Challenges in accommodating volume change of Si anodes for Li-ion batteries *ChemElectroChem* **2** 1645–51
[16] Ashuri M, He Q and Shaw L L 2016 Silicon as a potential anode material for Li-ion batteries: where size, geometry and structure matter *Nanoscale* **8** 74–103
[17] Chae S, Ko M, Kim K, Ahn K and Cho J 2017 Confronting issues of the practical implementation of Si anode in high-energy lithium-ion batteries *Joule* **1** 47–60
[18] Feng K, Li M, Liu W, Kashkooli A G, Xiao X, Cai M and Chen Z 2018 Silicon-based anodes for lithium-ion batteries: from fundamentals to practical applications *Small* **14** 1702737
[19] Li P, Zhao G, Zheng X, Xu X, Yao C, Sun W and Dou S X 2018 Recent progress on silicon-based anode materials for practical lithium-ion battery applications *Energy Storage Mater.* **15** 422–46
[20] Qi Y, Wang G, Li S, Liu T, Qiu J and Li H 2020 Recent progress of structural designs of silicon for performance-enhanced lithium-ion batteries *Chem. Eng. J.* **397** 125380
[21] Yuca N, Taskin O S and Arici E 2020 An overview on efforts to enhance the Si electrode stability for lithium ion batteries *Energy Storage* **2** e94
[22] Chen T, Wu J, Zhang Q and Su X 2017 Recent advancement of SiOx based anodes for lithium-ion batteries *J. Power Sources* **363** 126–44
[23] Xu Z L, Liu X, Luo Y, Zhou L and Kim J K 2017 Nanosilicon anodes for high performance rechargeable batteries *Prog. Mater. Sci.* **90** 1–44
[24] Mazouzi D, Karkar Z, Hernandez C R, Manero P J, Guyomard D, Roué L and Lestriez B 2015 Critical roles of binders and formulation at multiscales of silicon-based composite electrodes *J. Power Sources* **280** 533–49
[25] Holland A and He X 2021 Advanced Li-ion and beyond lithium batteries 2022–2032: technologies, players, trends, markets *IDTechEx* (available at: www.idtechex.com/en/research-report/advanced-li-ion-and-beyond-lithium-batteries-2022-2032-technologies-players-trends-markets/852)
[26] Lee B S, Son S B, Park K M, Seo J H, Lee S H, Choi I S, Oh K H and Yu W R 2012 Fabrication of Si core/C shell nanofibers and their electrochemical performances as a lithium-ion battery anode *J. Power Sources* **206** 267–73
[27] Wang M S, Song Y, Song W L and Fan L Z 2014 Three-dimensional porous carbon–silicon frameworks as high-performance anodes for lithium-ion batteries *ChemElectroChem* **1** 2124–30
[28] Jung C H, Choi J, Kim W S and Hong S H 2018 A nanopore-embedded graphitic carbon shell on silicon anode for high performance lithium ion batteries *J. Mater. Chem.* A **6** 8013–20
[29] Kim J M, Guccini V, Kim D, Oh J, Park S, Jeon Y, Hwang T, Salazar-Alvarez G and Piao Y 2018 A novel textile-like carbon wrapping for high-performance silicon anodes in lithium-ion batteries *J. Mater. Chem.* A **6** 12475–83
[30] Zhang X, Kong D, Li X and Zhi L 2019 Dimensionally designed carbon–silicon hybrids for lithium storage *Adv. Funct. Mater.* **29** 1806061
[31] Li X, Zhang M, Yuan S and Lu C 2020 Research progress of silicon/carbon anode materials for lithium-ion batteries: structure design and synthesis method *ChemElectroChem* **7** 4289–302
[32] Shi Q, Zhou J, Ullah S, Yang X, Tokarska K, Trzebicka B, Ta H Q and Rümmeli M H 2021 A review of recent developments in Si/C composite materials for Li-ion batteries *Energy Storage Mater.* **34** 735–54
[33] Manthiram A 2017 An outlook on lithium ion battery technology *ACS Cent. Sci.* **3** 1063–9
[34] Chen T, Thenuwara A C, Yao W, Sandoval S E, Wang C, Kang D H, Majumdar D, Gopalaswamy R and McDowell M T 2023 Benchmarking the degradation behavior of aluminum foil anodes for lithium-ion batteries *Batter. Supercaps* **6** e202200363

[35] Crowley P J, Scanlan K P and Manthiram A 2022 Diffusional lithium trapping as a failure mechanism of aluminum foil anodes in lithium-ion batteries *J. Power Sources* **546** 231973
[36] Heligman B T and Manthiram A 2021 Elemental foil anodes for lithium-ion batteries *ACS Energy Lett.* **6** 2666–72
[37] Santhosha A L, Medenbach L, Buchheim J R and Adelhelm P 2019 The indium−lithium electrode in solid-state lithium-ion batteries: phase formation, redox potentials, and interface stability *Batter. Supercaps* **2** 524–9
[38] Han S Y, Lewis J A, Shetty P P, Tippens J, Yeh D, Marchese T S and McDowell M T 2020 Porous metals from chemical dealloying for solid-state battery anodes *Chem. Mater.* **32** 2461–9
[39] Heligman B T, Kreder K J and Manthiram A 2019 Zn-Sn interdigitated eutectic alloy anodes with high volumetric capacity for lithium-ion batteries *Joule* **3** 1051–63
[40] Xu H, Li S, Zhang C, Chen X, Liu W, Zheng Y, Xie Y, Huang Y and Li J 2019 Roll-to-roll prelithiation of Sn foil anode suppresses gassing and enables stable full-cell cycling of lithium ion batteries *Energy Environ. Sci.* **12** 2991–3000
[41] Rhodes K J, Meisner R, Kirkham M, Dudney N and Daniel C 2012 *In situ* XRD of thin film tin electrodes for lithium ion batteries *J. Electrochem. Soc.* **159** A294–9
[42] Heligman B T, Scanlan K P and Manthiram A 2021 An in-depth analysis of the transformation of tin foil anodes during electrochemical cycling in lithium-ion batteries *J. Electrochem. Soc.* **168** 120544
[43] Li H, Yamaguchi T, Matsumoto S, Hoshikawa H, Kumagai T, Okamoto N L and Ichitsubo T 2020 Circumventing huge volume strain in alloy anodes of lithium batteries *Nat. Commun.* **11** 1584
[44] Ji B, Zhang F, Sheng M, Tong X and Tang Y 2017 A novel and generalized lithium-ion-battery configuration utilizing Al foil as both anode and current collector for enhanced energy density *Adv. Mater.* **29** 1604219
[45] Zhang M, Xiang L, Galluzzi M, Jiang C, Zhang S, Li J and Tang Y 2019 Uniform distribution of alloying/dealloying stress for high structural stability of an Al anode in high-areal-density lithium-ion batteries *Adv. Mater.* **31** 1900826
[46] Ryu J, Kang J, Kim H, Lee J H, Lee H and Park S 2020 Electrolyte-mediated nanograin intermetallic formation enables superionic conduction and electrode stability in rechargeable batteries *Energy Storage Mater.* **33** 164–72
[47] Chen S, Yang X, Zhang J, Ma J, Meng Y, Tao K, Li F and Geng J 2021 Aluminum−lithium alloy as a stable and reversible anode for lithium batteries *Electrochim. Acta* **368** 137626
[48] Sharma S S, Crowley P J and Manthiram A 2021 Aluminum–silicon alloy foils as low-cost, environmentally friendly anodes for lithium-ion batteries *ACS Sustain. Chem. Eng.* **9** 14515–24
[49] Kreder K J, Heligman B T and Manthiram A 2017 Interdigitated eutectic alloy foil anodes for rechargeable batteries *ACS Energy Lett.* **2** 2422–3
[50] Jung K N, Shin H S, Park M S and Lee J W 2019 Solid-state lithium batteries: bipolar design, fabrication, and electrochemistry *ChemElectroChem* **6** 3842–59
[51] Porz L, Swamy T, Sheldon B W, Rettenwander D, Frömling T, Thaman H L, Berendts S, Uecker R, Carter W C and Chiang Y M 2017 Mechanism of lithium metal penetration through inorganic solid electrolytes *Adv. Energy Mater.* **7** 1701003
[52] Sethuraman V A, Srinivasan V, Bower A F and Guduru P R 2010 *In situ* measurements of stress-potential coupling in lithiated silicon *J. Electrochem. Soc.* **157** A1253–61
[53] Rao B, Francis R and Christopher H 1977 Lithium-aluminum electrode *J. Electrochem. Soc.* **124** 1490–2
[54] Yazami R and Touzain P 1983 A reversible graphite-lithium negative electrode for electrochemical generators *J. Power Sources* **9** 365–71
[55] Yoshino A 2012 The birth of the lithium-ion battery *Angew. Chem., Int. Ed.* **51** 5798–800
[56] Nishio K and Furukawa N 2011 Practical batteries *Handbook of Battery Materials* Second, Completely Revised and Enlarged Edition ed C Daniel and J O Besenhard (Weinheim: Wiley-VCH Verlag GmbH & Co. KGaA) pp 27–85
[57] Sharma S K, Kim M S, Kim D Y and Yu J S 2013 Al nanorod thin films as anode electrode for Li ion rechargeable batteries *Electrochim. Acta* **87** 872–9
[58] Leite M S, Ruzmetov D, Li Z, Bendersky L A, Bartelt N C, Kolmakov A and Talin A A 2014 Insights into capacity loss mechanisms of all-solid-state Li-ion batteries with Al anodes *J. Mater. Chem.* A **2** 20552–9
[59] Oltean G, Tai C W, Edström K and Nyholm L 2014 On the origin of the capacity fading for aluminium negative electrodes in Li-ion batteries *J. Power Sources* **269** 266–73
[60] Doglione R, Vankova S, Amici J and Penazzi N 2017 Microstructure evolution and capacity: comparison between 2090-T8 aluminium alloy and pure aluminium anodes *J. Alloys Compd.* **727** 428–35
[61] Hudak N S and Huber D L 2011 Nanostructured lithium-aluminum alloy electrodes for lithium-ion batteries *ECS Trans.* **33** 1–13
[62] Hudak N S and Huber D L 2012 Size effects in the electrochemical alloying and cycling of electrodeposited aluminum with lithium *J. Electrochem. Soc.* **159** A688–95
[63] Kwon G D, Moyen E, Lee Y J, Joe J and Pribat D 2018 Graphene-coated aluminum thin film anodes for lithium-ion batteries *ACS Appl. Mater. Interfaces* **10** 29486–95
[64] Huang T S and Brittain J O 1987 The mechanical behavior of β-LiAl *Mater. Sci. Eng.* **93** 93–97
[65] Zheng T, Wang X, Jain E, Kramer D, Mönig R, Seita M and Boles S T 2020 Granular phase transformation of polycrystalline aluminum during electrochemical lithiation *Scr. Mater.* **188** 164–8
[66] Zheng T, Kramer D, Tahmasebi M H, Mönig R and Boles S T 2020 Improvement of the cycling performance of aluminum anodes through operando light microscopy and kinetic analysis *ChemSusChem* **13** 974–85
[67] Zheng T, Kramer D, Tahmasebi M H, Mönig R and Boles S T 2020 Exploring the reversibility of phase transformations in aluminum anodes through operando light microscopy and stress analysis *ChemSusChem* **13** 5910–20
[68] Liu Y, Hudak N S, Huber D L, Limmer S J, Sullivan J P and Huang J Y 2011 *In situ* transmission electron microscopy observation of pulverization of aluminum nanowires and evolution of the thin surface Al_2O_3 layers during lithiation–delithiation cycles *Nano Lett.* **11** 4188–94
[69] Maxell, Ltd 2017 Data sheet of lithium manganese dioxide rechargeable battery ML2032 (available at: https://biz.maxell.com/en/rechargeable_batteries/ML2032_DataSheet_17e.pdf)
[70] Wang H, Tan H, Luo X, Wang H, Ma T, Lv M, Song X, Jin S, Chang X and Li X 2020 The progress on aluminum-based anode materials for lithium-ion batteries *J. Mater. Chem.* A **8** 25649–62
[71] McAlister A J 1982 The Al−Li (aluminum−lithium) system *Bull. Alloy Phase Diagr.* **3** 177–83
[72] Massalski T B, Okamoto H, Subramanian P, Kacprzak L and Scott W W 1986 *Binary Alloy Phase Diagrams* (Metals Park, OH: American society for metals)
[73] Puhakainen K, Boström M, Groy T L and Häussermann U 2010 A new phase in the system lithium–aluminum: characterization of orthorhombic Li_2Al *J. Solid State Chem.* **183** 2528–33

[74] Okamoto H 2012 Al-Li (Aluminum-Lithium) *J. Phase Equilib. Diffus.* **33** 500–1
[75] Hamon Y, Brousse T, Jousse F, Topart P, Buvat P and Schleich D M 2001 Aluminum negative electrode in lithium ion batteries *J. Power Sources* **97–98** 185–7
[76] Li Q and Bjerrum N J 2002 Aluminum as anode for energy storage and conversion: a review *J. Power Sources* **110** 1–10
[77] Lindsay M J, Wang G X and Liu H K 2003 Al-based anode materials for Li-ion batteries *J. Power Sources* **119–121** 84–87
[78] Kishio K and Brittain J O 1979 Defect structure of β-LiAl *J. Phys. Chem. Solids* **40** 933–40
[79] Ghavidel M Z, Kupsta M R, Le J, Feygin E, Espitia A and Fleischauer M D 2019 Electrochemical formation of four Al-Li Phases (β-AlLi, Al_2Li_3, $AlLi_{2-x}$, Al_4Li_9) at intermediate temperatures *J. Electrochem. Soc.* **166** A4034–40
[80] Tahmasebi M H, Kramer D, Mönig R and Boles S T 2019 Insights into phase transformations and degradation mechanisms in aluminum anodes for lithium-ion batteries *J. Electrochem. Soc.* **166** A5001–7
[81] Zhang X, Zhao W, Cai J, Xu C, Chen S, Chen G and Wang G 2022 Solid electrolyte interphase layer induced electrochemical behavior diversity of aluminum foil anode for lithium ion batteries *Solid State Ion.* **387** 116081
[82] Wen C J, Boukamp B, Huggins R A and Weppner W 1979 Thermodynamic and mass transport properties of "LiAl" *J. Electrochem. Soc.* **126** 2258–66
[83] Wen C J, Weppner W, Boukamp B and Huggins R A 1980 Electrochemical investigation of solubility and chemical diffusion of lithium in aluminum *Metall. Trans.* B **11** 131–7
[84] Tokuhiro T, Susmam S, Brun T O and Volin K J 1989 ^{7}Li NMR relaxation in supreionic β-lithium aluminum *J. Phys. Soc. Japan* **58** 2553–69
[85] Zhang J, Zheng T, Lam K H and Boles S T 2023 Design considerations and cycling guidance for aluminum foil anodes in lithium-ion rechargeable cells *Electrochim. Acta* **456** 142437
[86] Kellington S H, Loveridge D and Titman J M 1969 The lattice parameters of some alloys of lithium *J. Phys. D: Appl. Phys.* **2** 1162
[87] Kim M S, Deepika Lee S H, Kim M S, Ryu J H, Lee K R, Archer L A and Cho W I 2019 Enabling reversible redox reactions in electrochemical cells using protected LiAl intermetallics as lithium metal anodes *Sci. Adv.* **5** eaax5587
[88] Qi Y, Hector L G, James C and Kim K J 2014 Lithium concentration dependent elastic properties of battery electrode materials from first principles calculations *J. Electrochem. Soc.* **161** F3010
[89] Sarmiento-Pérez R, Cerqueira T F T, Valencia-Jaime I, Amsler M, Goedecker S, Romero A H, Botti S and Marques M A L 2015 Novel phases of lithium-aluminum binaries from first-principles structural search *J. Chem. Phys.* **142** 024710
[90] Geronov Y, Zlatilova P and Staikov G 1984 The secondary lithium—aluminium electrode at room temperature: II. Kinetics of the electrochemical formation of the lithium—aluminium alloy *J. Power Sources* **12** 155–65
[91] Melendres C A 1977 Kinetics of electrochemical incorporation of lithium into aluminum *J. Electrochem. Soc.* **124** 650–5
[92] Noble B, Harris S J and Dinsdale K 1982 The elastic modulus of aluminium-lithium alloys *J. Mater. Sci.* **17** 461–8
[93] Baranski A and Fawcett W 1982 The formation of lithium-aluminum alloys at an aluminum electrode in propylene carbonate *J. Electrochem. Soc.* **129** 901–7
[94] Geronov Y, Zlatilova P and Moshtev R V 1984 The secondary lithium—aluminium electrode at room temperature: I. Cycling in $LiClO_4$—propylene carbonate solutions *J. Power Sources* **12** 145–53
[95] Wang C, Meng Y, Ceder G and Li Y 2008 Electrochemical properties of nanostructured $Al_{1-x}Cu_x$ alloys as anode materials for rechargeable lithium-ion batteries *J. Electrochem. Soc.* **155** A615–22
[96] Geronov Y, Zlatilova P and Staikov G 1984 Electrochemical nucleation and growth of β-LiAl alloy in aprotic electrolyte solutions *Electrochim. Acta* **29** 551–5
[97] Callister W D and Rethwisch D G 2018 *Materials Science and Engineering: An Introduction* vol 9 (New York: Wiley)
[98] Huggins R A 1999 Lithium alloy negative electrodes *J. Power Sources* **81–82** 13–19
[99] Zhang W J 2011 Lithium insertion/extraction mechanism in alloy anodes for lithium-ion batteries *J. Power Sources* **196** 877–85
[100] Miao J and Thompson C V 2018 Kinetic study of the initial lithiation of amorphous silicon thin film anodes *J. Electrochem. Soc.* **165** A650–6
[101] Miao J, Wang B and Thompson C V 2020 Kinetic study of lithiation-induced phase transitions in amorphous germanium thin films *J. Electrochem. Soc.* **167** 090557
[102] Deal B E and Grove A S 1965 General relationship for the thermal oxidation of silicon *J. Appl. Phys.* **36** 3770–8
[103] Avrami M 1939 Kinetics of phase change. I general theory *J. Chem. Phys.* **7** 1103–12
[104] Avrami M 1940 Kinetics of phase change. II transformation-time relations for random distribution of nuclei *J. Chem. Phys.* **8** 212–24
[105] Avrami M 1941 Granulation, phase change, and microstructure kinetics of phase change. III *J. Chem. Phys.* **9** 177–84
[106] Chan A K, Tatara R, Feng S, Karayaylali P, Lopez J, Stephens I E L and Shao-Horn Y 2019 Concentrated electrolytes for enhanced stability of Al-alloy negative electrodes in Li-ion batteries *J. Electrochem. Soc.* **166** A1867–74
[107] Qin B, Jeong S, Zhang H, Ulissi U, Carvalho D V, Varzi A and Passerini S 2019 Enabling reversible (De)lithiation of aluminum by using bis(fluorosulfonyl)imide-based electrolytes *ChemSusChem* **12** 208–12
[108] Li S, Niu J, Zhao Y C, So K P, Wang C, Wang C A and Li J 2015 High-rate aluminium yolk-shell nanoparticle anode for Li-ion battery with long cycle life and ultrahigh capacity *Nat. Commun.* **6** 7872
[109] Qin B, Diemant T, Zhang H, Hoefling A, Behm R J, Tübke J, Varzi A and Passerini S 2019 Revisiting the electrochemical lithiation mechanism of aluminum and the role of li-rich phases ($Li_{1+x}Al$) on capacity fading *ChemSusChem* **12** 2609–19
[110] Al-Obeidi A, Kramer D, Thompson C V and Mönig R 2015 Mechanical stresses and morphology evolution in germanium thin film electrodes during lithiation and delithiation *J. Power Sources* **297** 472–80
[111] Al-Obeidi A, Kramer D, Boles S T, Mönig R and Thompson C V 2016 Mechanical measurements on lithium phosphorous oxynitride coated silicon thin film electrodes for lithium-ion batteries during lithiation and delithiation *Appl. Phys. Lett.* **109** 071902
[112] Pharr M, Choi Y S, Lee D, Oh K H and Vlassak J J 2016 Measurements of stress and fracture in germanium electrodes of lithium-ion batteries during electrochemical lithiation and delithiation *J. Power Sources* **304** 164–9
[113] Al-Obeidi A, Kramer D, Mönig R and Thompson C V 2016 Mechanical stresses and crystallization of lithium phosphorous oxynitride-coated germanium electrodes during lithiation and delithiation *J. Power Sources* **306** 817–25
[114] Guidotti R A and Masset P J 2008 Thermally activated ("thermal") battery technology: part IV. Anode materials *J. Power Sources* **183** 388–98
[115] Huang T S and Brittain J O 1982 Effect of defect structure upon the mechanical behavior of β-LiAl through dislocation damping and hardness studies *Metall. Trans.* A **13** 2173–6

[116] Ali H, Khan H A and Pecht M G 2020 Evaluation of Li-based battery current, voltage, and temperature profiles for in-service mobile phones *IEEE Access* **8** 73665–76
[117] PANASONIC LTD 2023 Li ion rechargeable batteries specifications for NCR18650BF (available at: https://api.pim.na.industrial.panasonic.com/file_stream/main/fileversion/3446)
[118] Zheng T, Zhang J, Jin W and Boles S T 2023 Utilization of Li-rich phases in aluminum anodes for improved cycling performance through strategic thermal control *ACS Appl. Energy Mater.* **6** 1845–52
[119] LePan N 2020 All the world's metals and minerals in one visualization (available at: www.visualcapitalist.com/all-the-worlds-metals-and-minerals-in-one-visualization)
[120] U.S. Department of the Interior and U.S. Geological Survey 2023 Mineral commodity summaries 2023 (available at: https://pubs.usgs.gov/periodicals/mcs2023/mcs2023.pdf)
[121] Chen Q and Sieradzki K 2013 Spontaneous evolution of bicontinuous nanostructures in dealloyed Li-based systems *Nat. Mater.* **12** 1102
[122] Weissmüller J and Sieradzki K 2018 Dealloyed nanoporous materials with interface-controlled behavior *MRS Bull.* **43** 14–19
[123] Abe I, Horiba T, Abe Y, Hida K, Matsuyama T, Yasuno S and Komaba S 2020 Investigation and improvement of metallic aluminum as alloying electrode in non-aqueous Li cells *J. Electrochem. Soc.* **167** 110513
[124] Badwe N, Chen X and Sieradzki K 2017 Mechanical properties of nanoporous gold in tension *Acta Mater.* **129** 251–8
[125] Li R and Sieradzki K 1992 Ductile-brittle transition in random porous Au *Phys. Rev. Lett.* **68** 1168–71
[126] Huang Y, Liu C, Wei F, Wang G, Xiao L, Lu J and Zhuang L 2020 Chemical prelithiation of Al for use as an ambient air compatible and polysulfide resistant anode for Li-ion/S batteries *J. Mater. Chem.* A **8** 18715–20
[127] Fan H, Li S, Yu Y, Xu H, Jiang M, Huang Y and Li J 2021 Air-stable Li_xAl foil as free-standing electrode with improved electrochemical ductility by shot-peening treatment *Adv. Funct. Mater.* **31** 2100978
[128] Desai P, Huang J, Foix D, Tarascon J M and Mariyappan S 2022 Zero volt storage of Na-ion batteries: performance dependence on cell chemistry! *J. Power Sources* **551** 232177
[129] Ou X, Zhang G, Zhang S, Tong X and Tang Y 2020 Simultaneously pre-alloying and artificial solid electrolyte interface towards highly stable aluminum anode for high-performance Li hybrid capacitor *Energy Storage Mater.* **28** 357–63
[130] Ui K, Yamamoto K, Ishikawa K, Minami T, Takeuchi K, Itagaki M, Watanabe K and Koura N 2009 Development of non-flammable lithium secondary battery with room-temperature ionic liquid electrolyte: performance of electroplated Al film negative electrode *J. Power Sources* **183** 347–50
[131] Au M, McWhorter S, Ajo H, Adams T, Zhao Y and Gibbs J 2010 Free standing aluminum nanostructures as anodes for Li-ion rechargeable batteries *J. Power Sources* **195** 3333–7
[132] Kim Y, Ha K H, Oh S M and Lee K T 2014 High-capacity anode materials for sodium-ion batteries *Chem. Eur. J.* **20** 11980–92
[133] Sakka Y, Yamashige H, Watanabe A, Takeuchi A, Uesugi M, Uesugi K and Orikasa Y 2022 Pressure dependence on the three-dimensional structure of a composite electrode in an all-solid-state battery *J. Mater. Chem.* A **10** 16602–9
[134] Zhang Z, Dong K, Mazzio K A, Hilger A, Markötter H, Wilde F, Heinemann T, Manke I and Adelhelm P 2023 Phase transformation and microstructural evolution of CuS electrodes in solid-state batteries probed by *in situ* 3D x-ray tomography *Adv. Energy Mater.* **13** 2203143
[135] Albero Blanquer L, Marchini F, Seitz J R, Daher N, Bétermier F, Huang J, Gervillié C and Tarascon J M 2022 Optical sensors for operando stress monitoring in lithium-based batteries containing solid-state or liquid electrolytes *Nat. Commun.* **13** 1153